

**Development and Validation of a Time-lag Correction for
Vaisala Radiosonde Humidity Measurements**

by

Larry M. Miloshevich
National Center for Atmospheric Research*
Boulder, Colorado

Ari Paukkunen
Vaisala Oy
Helsinki, Finland

Holger Vömel and Samuel J. Oltmans
National Oceanic and Atmospheric Administration
Boulder, Colorado

*The National Center for Atmospheric Research (NCAR) is sponsored by the National Science Foundation.

ABSTRACT

This study presents a method of improving the accuracy of relative humidity (RH) measurements from Vaisala RS80 and RS90 radiosondes, by applying sensor-based corrections for well-understood sources of measurement error. Laboratory measurements of the sensor time-constant as a function of temperature are used to develop a correction for time-lag error that results from slow sensor response at cold temperatures. The time-lag correction is a numerical inversion algorithm that calculates the ambient (“true”) humidity profile from the measured humidity and temperature profiles, based on the sensor time-constant. Existing corrections for two sources of dry bias error in RS80 humidity measurements are also included in the correction procedure: inaccuracy in the sensor calibration at cold temperatures, and chemical contamination of sensors manufactured before June 2000 by non-water molecules from the radiosonde packaging material.

The correction procedure was evaluated by comparing corrected RS80-H measurements with simultaneous measurements from the reference-quality NOAA/CMDL balloon-borne cryogenic hygrometer. The time-lag correction is shown to recover vertical structure in the humidity profile that had been “smoothed” by the slow sensor response, especially in the upper troposphere and lower stratosphere, revealing a much sharper troposphere-stratosphere transition than is apparent in the original measurements. The corrections reduced the mean dry bias in the radiosonde measurements relative to the hygrometer from 4 %RH at -20°C and 10 %RH at -70°C to about ± 2 %RH at all temperatures, and the variability at cold temperatures is substantially reduced. A shortcoming of the existing contamination correction is also uncovered, and a modification is suggested. The impact of the corrections on several radiosonde datasets is shown.

Development and Validation of a Time-lag Correction for Vaisala Radiosonde Humidity Measurements

1. Introduction

Radiosonde relative humidity (RH) measurements are used in a wide variety of operational and research applications, including initializing and evaluating numerical models, validating remote-sensor water vapor retrievals, constructing water vapor climatologies, studying climate trends, parameterizing water vapor and cloud processes, and performing radiative transfer calculations. Radiosonde data have traditionally been used operationally for weather forecasting, but more recent climate-related uses have placed greater demands for accuracy on radiosonde humidity data, particularly in the challenging measurement environment of cold temperatures and low water vapor concentrations in the upper troposphere (UT) and lower stratosphere (LS). The accuracy of radiosonde humidity measurements in the UT/LS region is not well documented.

Most operational radiosonde humidity data are not suitable for climate-related research unless great care is taken to understand both the measurement characteristics of the specific radiosondes used, and changes over time in the data processing and reporting practices of individual radiosonde stations (Elliott and Gaffen 1991). A comparison of global radiosonde humidity measurements with satellite water vapor retrievals as a common standard (Soden and Lanzante 1996) found large shifts that often fell along geopolitical boundaries of countries that use different radiosonde types. The U.S. National Weather Service (NWS) currently uses a mix of Vaisala RS80-H radiosondes with thin-film capacitance humidity sensors, and Sippican (formerly VIZ) B2 radiosondes with carbon hygistor humidity sensors. The change from VIZ to Vaisala radiosondes at some NWS stations in 1995 and 1998 produced the appearance of climate shifts that varied with altitude, season, and geographic location (Elliott et al. 2002). Ross and Gaffen (1998) have suggested that apparent atmospheric drying in the tropics observed by Schroeder and McGuirk (1998), which used satellite data calibrated with radiosonde data, may in fact be the result of changes in radiosonde instrumentation. Climate trends derived from radiosonde data are suspect unless the radiosonde measurement characteristics are carefully

considered, and even soundings from the same source (e.g., NWS) are not of equal reliability, especially in the UT.

Vaisala radiosondes are the most frequently used radiosondes in the world, and numerous studies have investigated their measurement accuracy, both directly and indirectly. A systematic dry bias in Vaisala RS80 humidity measurements has been noted in comparison to Raman lidar measurements (Ferrare et al. 1995) and satellite water vapor retrievals (Soden and Lanzante 1996), and in underpredicting clouds and precipitation in a Numerical Weather Prediction model (Lorenc et al. 1996). Zipser and Johnson (1998) frequently observed unrealistically dry tropical boundary layers during TOGA COARE (Tropical Oceans Global Atmosphere Coupled Ocean Atmosphere Response Experiment) in 1992-1993. Heymsfield and Miloshevich (1995) observed substantially ice-subsaturated humidities in cirrus clouds when simultaneous ice crystal measurements indicated that the crystals were pristine and therefore actively growing in an ice-supersaturated environment. Turner et al. (2003) and Revercomb et al. (2003) used dual-radiosonde launches at the Department of Energy (DOE) Atmospheric Radiation Measurement (ARM) program's Oklahoma site between 1996 and 2000 to show that RS80-H radiosonde pairs were biased from each other by an amount that differs between calibration batches and within the same batch.

Vaisala and the National Center for Atmospheric Research (NCAR) identified physical causes of the dry bias and developed sensor-based corrections for RS80 radiosondes (Wang et al. 2002, hereafter "W02"). A statistical temperature-dependent correction for RS80-A humidity measurements was developed by Miloshevich et al. (2001, hereafter "M01") based on dual soundings with the reference-quality cryogenic frostpoint hygrometer operated by the National Oceanic and Atmospheric Administration Climate Modeling and Diagnostics Laboratory (NOAA/CMDL). Turner et al. (2003) developed an empirical correction approach that scales the radiosonde measurements with a constant factor that matches the total-column Precipitable Water (PW) with that measured by a microwave radiometer (MWR). The MWR scaling was shown from independent measurements to improve the accuracy of the radiosonde humidity measurements, but its impact is primarily limited to the lower troposphere (where most of the PW resides), rather than the UT where measurement errors are larger and more complicated.

The aim of the present study is to further improve the accuracy of Vaisala radiosonde humidity measurements, particularly in the UT, by developing and validating a method to correct the time-lag error that results from slow sensor response to changes in the ambient humidity at cold temperatures. Section 2 of this paper describes Vaisala radiosonde humidity sensors and existing corrections for RS80 bias errors. A method of correcting the measurements for time-lag error is developed in Section 3. The combined time-lag and bias corrections are evaluated in Section 4 by comparing corrected radiosonde measurements to simultaneous measurements from the NOAA/CMDL cryogenic hygrometer. The impact of the corrections on several radiosonde datasets is shown in Section 5.

2. Sensor Principles and Bias Errors

Vaisala thin-film capacitance humidity sensors consist of a thin polymer layer between the porous electrodes of a capacitor. Water molecules diffuse through the electrode and are captured at binding sites within the polymer structure in concentrations proportional to the ambient water vapor density, altering the capacitance that is measured by the radiosonde. A calibration curve for the sensor response at +20°C converts the measured capacitance to RH with respect to liquid water if the temperature was +20°C (U_{20}). A second calibration curve adjusts U_{20} for the temperature-dependence of the sensors to yield the measured humidity at the ambient temperature (U_m). Additional details of the sensor principles and calibration are given by M01.

Vaisala currently produces four types of radiosondes: the RS80-A introduced in 1980, the RS80-H introduced in 1992, the RS90 introduced in 2000, and the RS92 released in October 2003. The RS80-A is still the most widely used operational radiosonde in the world today, and the RS80-H is widely used in the U.S., the U.K., and by many research programs. The RS90 is less widely used, but was adopted by the DOE/ARM program in 2001. Each sensor type has different response characteristics due to different sensor polymer composition and chemistry (A vs H), different physical size and thickness of the polymer layer, and different calibration accuracy. The RS90 and RS92 use the H-type polymer, but the size and thickness of the polymer layer is smaller than the RS80-H, which improves the sensor response time. It is

imperative to distinguish between the sensor types when considering the accuracy of the measurements, and when applying corrections for measurement errors. In general, all Vaisala radiosonde humidity sensors are qualitatively subject to the same types of measurement errors, but the magnitude of each error varies considerably between the sensor types. Furthermore, the sensor characteristics and corrections discussed in this paper do not apply at all to non-Vaisala sensors.

Several sources of bias error have been identified in RS80-A and RS80-H humidity measurements (see W02 and M01). Corrections for the two primary sources of RS80 bias error, known as “temperature-dependence error” and “contamination error”, will be incorporated into the time-lag correction that is developed in Section 3. The RS80 bias errors are summarized below, and the published corrections are shown in Figure 1. The performance of these bias corrections, and comparison of corrected radiosonde data with other coincident water vapor measurements, is reported by Revercomb et al. (2003), Turner et al. (2003), Soden et al. (2004), and Ferrare et al. (2004).

- Temperature-dependence (TD) error arises from inaccuracy in the calibration model for the temperature-dependence of the sensor response. This is not an inherent limitation of the sensor, and the correction simply reflects a more accurate calibration model at low temperatures. The correction is essentially zero above -20°C and increases with decreasing temperature. The correction is considerably greater for the RS80-A than the RS80-H (e.g., at -60°C the RS80-H correction is 12% of the measured RH, but the RS80-A correction is 75% of the measured RH). No TD correction is applied to RS90 or RS92 data because the calibration procedure is more accurate (Paukkunen et al. 2001).
- Contamination error arises from the tendency of non-water molecules, mainly from plastics in the radiosonde packaging material, to occupy binding sites in the sensor polymer and render them unavailable to water molecules, leading to a dry bias in the measurements. Evaluation of radiosondes of various ages (W02) led to a statistical correction that is a function of the basic calibration humidity (U_{20}) and the age of the radiosonde. The bottom panels in Fig. 1 show that the H-polymer is much more susceptible to contamination than the A-polymer. This statistical

correction approach reduces the mean dry bias, but it cannot account for substantial variability in the contamination rate caused by factors such as the temperature at which the radiosondes are stored. The desiccant type shipped with radiosondes was changed in Sept. 1998, which is thought to reduce the contamination by 30-50% (W02). The contamination correction for individual RS80 radiosondes can be improved by using coincident surface RH measurements from a reference-quality instrument (W02), if care is taken that solar heating does not affect the radiosonde or reference sensor when the comparison is made. The contamination problem was reduced or eliminated for RS80 radiosondes produced after 1 June 2000 when Vaisala began shipping radiosondes with a sealed sensor cap that is removed just prior to launch. No contamination correction has been investigated for the RS90 because the error is thought to be much smaller due to the replacement of styrofoam in the radiosonde construction by cardboard. The RS92 radiosonde addresses the contamination problem using “regeneration,” where the sensor is heated prior to launch to drive off contaminants and recover the original calibration (Hirvensalo et al. 2002).

The TD and contamination corrections must be applied in a particular manner, which is different for the two RS80 radiosonde types. Since contamination affects the basic humidity calibration (U_{20}), the original (inaccurate) calibration for the temperature-dependence of the sensor must first be removed from the measured humidity U_m to recover U_{20} [W02, Eq. (5.1), where $U_{20}=f(U_m, T)$]. The contamination correction (ΔU_{20}) is then calculated from polynomial functions (p_1 and p_2) of U_{20} and the radiosonde age [W02, Eq. (4.1), where $\Delta U_{20}=p_1(U_{20})*p_2(age)$, but $\Delta U_{20}=0$ for radiosondes manufactured after 1 June 2000, and ΔU_{20} is reduced by 30% for radiosondes produced after September 1998 when the desiccant type was changed]. The radiosonde age is the time between its calibration and launch, and the calibration date can be determined from the radiosonde serial number as described in Appendix A. If the radiosonde is an RS80-H, then the TD correction simply involves applying the more accurate TD calibration equation to the contamination-corrected U_{20} , to recover the corrected humidity at the ambient temperature [W02, Eq. (5.2-H), where $U_m=f(U_{20}+\Delta U_{20}, T)$]. The RS80-A is treated differently, because the TD correction is applied directly to the measurements (U_m , not U_{20}). The original (inaccurate) RS80-A TD calibration equation is applied to recover the measured humidity

corrected for only the contamination error [W02, Eq. (5.2-A)], then this result is multiplied by the TD correction factor [M01, Eq. (4)].

3. Development of the Time-Lag Correction

Time-lag error results from the sensor's non-zero response time to changes in the ambient humidity, when water molecules diffuse into or out of the sensor polymer as the sensor strives to maintain equilibrium with the environment. The time-response of a sensor is typically described by its time-constant (τ), which is the time required for the sensor to respond to 63% of an instantaneous change in the ambient humidity. This section presents laboratory measurements of the sensor time-constant as a function of temperature, followed by development of a numerical inversion algorithm that calculates the ambient ("true") humidity profile from the measured humidity and temperature profiles based on the time-constant measurements.

a. Time-constant measurements

Vaisala conducted laboratory measurements of the response time for their radiosonde humidity sensors over the temperature range +25 to -60°C . The experimental technique involved exposing each sensor to an essentially instantaneous step-change in humidity by rapidly switching between temperature-stabilized dry and moist flows directed at the sensor. The dry flow is dry nitrogen (0 %RH), and the moist flow is at a humidity that is near water-saturation above 0°C and near ice-saturation below 0°C . Rapid measurements of the sensor output are made at 5-120 ms intervals, depending on the temperature. Both the sensor time-constant (τ) and the 90% response time were determined. The time-constant is measured under conditions of both increasing and decreasing RH, as there may be differences in the rate at which the sensor polymer absorbs or desorbs water molecules. Seven sensors of each type were tested at six temperatures for both increasing and decreasing RH, and each test was repeated twice in order to investigate the experimental uncertainty.

The mean and standard deviation of the time-constant measurements are shown in Figure 2, and are given in Table 1 as a function of temperature, sensor type, and direction of humidity

change (increasing vs decreasing). The coefficients of the polynomial fits in Fig. 2 that give the temperature-dependence of the time-constant used in the correction procedure, $\tau(T)$, are given in Table 2. The time-constant increases approximately exponentially with decreasing temperature. The RS90 responds considerably faster than the RS80-H even though both sensors use the H-type polymer, mainly because the polymer layer is thinner in the RS90 sensor. The A-type polymer is more sensitive (responds faster) than the H-type polymer. Time-lag error begins to affect the sensor's ability to discern detailed vertical structure in the humidity profile when the time-constant exceeds about 20 s (100 m of radiosonde ascent), and this threshold is reached at a temperature of -43°C for RS80-A, -34°C for RS80-H, and -47°C for RS90. Note that the time-constant values given by extrapolation of the polynomial fits below the lowest measurement temperature of -60°C are increasingly uncertain with decreasing temperature, and a conservative extrapolation was chosen to favor undercorrection rather than overcorrection.

The use of polynomial fits to the mean values introduces curve fit error, whose magnitude varies with the temperature. In addition, the time-constant will be faster (smaller) than the mean value for 50% of radiosondes, and a conservative approach of using time-constant values that are one standard deviation below the mean is used to avoid overcorrection for some radiosondes. The time-constant values calculated from the polynomial fits are adjusted by a factor $F(T)$ that eliminates the curve fit error and decreases the time-constant by one standard deviation at the measurement temperatures. These adjustment factors are given in Table 3. The time-constant expression used in the correction algorithm is then given by:

$$\tau(T) = 10^{P(T)} \times F(T), \quad (1)$$

where $P(T)$ is the appropriate polynomial fit evaluated at temperature T , and $F(T)$ is given by linear interpolation of the adjustment factors in Table 3 to temperature T . The advantage of applying adjustment factors to the polynomial fits rather than just using linear interpolation of the time-constant measurements directly is that the resulting temperature-dependence retains the underlying smoothness of the polynomial fit.

b. Mathematical basis of the time-lag correction

Inspection of the high-rate time constant measurements indicated that Vaisala humidity sensors respond approximately exponentially to a change in RH, as described by the common “growth-law equation:”

$$\frac{dU_m}{dt} = k \cdot (U_a - U_m), \quad (2)$$

where U_m is the instantaneous *measured* RH, U_a is the *ambient* (“true”) RH that is driving the change in U_m , and k is a constant. The solution of this equation for a step-change in U_a at time $t=t_o$ gives the measured RH as a function of time:

$$U_m(t) = U_a - (U_a - U_m(t_o)) \cdot e^{-\Delta t/\tau}, \quad (3)$$

where $\tau=1/k$ is the 63% response time, and $\Delta t=t-t_o$. It can be shown from Eq. (3) that the fractional response of the sensor as a function of time is given by $1 - e^{-\Delta t/\tau}$ (Fig. 3). For ideal exponential response, the 90% response time is a factor of 2.3 greater than the time-constant, and this ratio of the 90% to 63% response time from the time-constant measurements is shown in Fig. 4. Most points are in the relatively narrow range 2.1-2.7. The outlying RS90 point at -20°C is thought to have resulted from experimental error, but this uncertainty will not noticeably affect the time-lag correction because the RS90 responds very fast at -20°C ($\tau=2$ s). Apart from two outlying points at -60°C for the RS80-A and RS90, the sensor response is reasonably consistent with the exponential behavior implicit in Eq. (2), although non-exponential sensor behavior must be acknowledged as a source of uncertainty in the time-lag correction.

The time-lag effect and its dependence on temperature and sensor type are illustrated in Fig. 5, which simulates the humidity profile that would be measured for a specified ambient humidity profile, based on Eq. (3). The time-lag effect is small at temperatures warmer than about -40°C , but is appreciable at -60°C or colder, most notably for the RS80-H. The additional vertical distance required for the measurements to reach the final ambient humidity at -60°C is about 1 km for the RS80-A and RS90, and >3 km for the RS80-H. In addition to temperature, the time-

lag effect is sensitive to the ambient humidity gradient (the humidity gradient shown in Fig. 5 is moderately steep but quite common in the atmosphere).

The essence of the time-lag correction involves solving Eq. (3) for the ambient humidity U_a in terms of the measured humidity $U_m(t)$. The sample spacing Δt must be sufficiently short that U_a can be treated as constant during each timestep, as is assumed in Eq. (3). Experience with many atmospheric profiles has shown that timesteps up to at least 10 s meet this condition, even for very steep humidity gradients. Rearranging Eq. (3), the ambient humidity required to drive the measured humidity from its value at the beginning of the timestep, $U_m(t_o)$, to its value at the end of the timestep, $U_m(t_f)$, is given by:

$$U_c = \frac{U_m(t_f) - (U_m(t_o) \cdot X)}{1 - X}, \quad (4)$$

where $X \equiv e^{-\Delta t/\tau}$, and the “ambient” humidity U_a will henceforth be referred to as the “corrected” humidity U_c . Note that data which are not time-resolved (e.g., NWS “mandatory and significant levels” data) cannot be corrected for time-lag error.

c. Numerical implementation of the time-lag correction

Correction of Vaisala radiosonde humidity data for time-lag error involves applying Eq. (4) sequentially to each timestep in a humidity profile, where the change in the measured humidity, U_m , during the timestep dictates the ambient (corrected) humidity, U_c , that must have driven that change. Since Eqs. (3) and (4) are self-consistent, the ambient humidity profile in Fig. 5 (bold curve) can be precisely recovered from any of the nine measured profiles shown (smooth curves), given the temperature and sensor type. Unfortunately, it is not so straightforward when real data are considered.

Vaisala RH data are typically recorded with a resolution (precision) of 1 %RH, where U_m is constant for some time period followed by an abrupt change of 1 %RH during a single timestep. The measured RS80-H humidity profile shown in Fig. 6 illustrates the time-lag correction

procedure, where the original 1 %RH resolution data (black stairsteps) are first smoothed (blue, U_m), then the time-lag correction is applied to U_m to recover the ambient (corrected) RH profile (red, U_c). Direct application of Eq. (4) to 1 %RH resolution measurements (Fig. 6a) fails for two reasons. During the periods when U_m is constant, U_c must equal U_m because otherwise there would be a humidity difference to drive some change in U_m . Second, the abrupt large changes in U_m by 1 %RH produces large spikes in U_c , because the ambient humidity must be very different from U_m to drive such a rapid (apparent) change in U_m at cold temperatures, when the time-constant is relatively large compared to the 6 s timestep. A primary requirement of the time-lag correction is that it operate on a physically realistic time-series (not stairsteps), which necessitates some type of smoothing for low-resolution data (higher-resolution 0.1 %RH data is discussed in section 3e), as well as good data quality control to remove instrument-related noise and artifacts from the raw data processing. Several smoothing approaches were investigated, including boxcar average, polynomial fitting, and Fourier and wavelet techniques, but none of these provide suitable smoothing that also constrains the smoothed data to be consistent with the original data to within the measurement resolution for features of all scales. Appendix B describes a new derivative-based smoothing technique that assures consistency between the smoothed and original measurements to within a specified tolerance.

The time-lag correction procedure is a sequence of 4 steps illustrated in Fig. 6b-e. The first step is to construct a “skeleton” of the measured profile that is defined by a single point in the center of each constant-RH period, with additional points near the ends of long constant periods to better define the shape of the profile (Fig. 6b, U_m). Although the skeleton profile appears reasonably smooth, the corrected profile calculated from Eq. (4) (U_c , red) is much less smooth because tiny changes in slope at the U_m skeleton points are amplified in proportion to the time-constant. The original measurements contain no information on the precise shape of the profile on scales smaller than the length of the constant periods, so each skeleton point is assigned an “uncertainty” or “tolerance”, and is allowed to move within this range. The smoothing technique described in Appendix B is designed to minimize the third derivative of a time-series (i.e., minimize changes in the curvature), where each point is adjustable only within its specified tolerance range. This smoothing algorithm is applied to the skeleton U_m profile (Fig. 6c) with a tolerance of ± 0.15 %RH for most points (± 0.5 %RH for points added near the edges of long

constant periods). The resulting U_c profile is markedly smoother, while ensuring that the smoothed U_m skeleton remains consistent with the original measurements within the smoothing tolerance. The smoothing tolerance values were chosen by experimentation to achieve smooth results while ensuring that the total smoothing from multiple smoothing operations affects the data by a maximum amount that is smaller than the resolution of the measurements. This derivative-based smoothing algorithm is central to the time-lag correction procedure, and may have broader application for the smoothing of time-series data within specified constraints (such as an uncertainty estimate). Its numerical implementation and sensitivity to the smoothing tolerance parameter are described in Appendix B.

A smooth measured profile does not necessarily produce a corrected profile that is equally smooth, due to the complicated exponential relationship between U_m and U_c . Assuming that an ambient humidity profile is inherently smooth (in a derivative-sense), the corresponding measured profile will not be precisely smooth because it is merely the sensor response to a smooth ambient profile via Eq. (3). Since U_c is very sensitive to the slope of U_m at cold temperatures, a small change in a given U_m point can produce a large change in the corresponding U_c point (and vice versa). A modified version of the smoothing algorithm is applied to the U_c profile, which iteratively adjusts and maximizes the smoothing tolerance for individual U_c points such that no U_m point moves by more than a specified amount. The smoothed U_c profile from this second smoothing operation is shown in Fig. 6d for smoothing tolerance parameter $\Delta U_m = \pm 0.15$ %RH. The implementation of the modified smoothing algorithm is described in Appendix B.

At this point in the time-lag correction procedure (Fig. 6d), the skeleton U_m profile is consistent with the original measurements at the skeleton points by a known and controlled amount, ± 0.3 %RH for most points (± 0.15 %RH from the first smoothing step, and ± 0.15 %RH from the second smoothing step). The time-lag correction is essentially complete except for restoring the original 6 s time-series. In most cases it would be sufficient to apply spline or polynomial interpolation to the smoothed U_m profile followed by calculation of the final U_c profile, but occasionally spline interpolation produces undesirable artifacts when the slope changes abruptly. The technique used in Fig. 6e to restore the full time-series uses the

smoothing algorithm to repeatedly add points to the U_m profile midway between the existing skeleton points, where the existing points are held fixed (tolerance = 0) and the new points are assigned a large tolerance such that they will conform smoothly to the established U_m profile. Several iterations of new points produces a U_m profile of sufficient point density that spline interpolation can safely be used to fully restore the original time-series and calculate the final U_c profile.

The smoothing tolerance parameter controls how “tightly” the smoothed U_m profile is tied to the skeleton of the original measurements, which affects the shape of the U_c profile and is therefore a source of uncertainty. Figure 6e (dashed) shows the sensitivity of U_c to the smoothing tolerance by comparing U_c using the example (standard) smoothing tolerance ($\Delta U_m = \pm 0.15$) with U_c when the smoothing is either substantially less ($\Delta U_m = \pm 0.05$), or substantially more ($\Delta U_m = \pm 0.3$). The uncertainty due to the smoothing choice is negligible for most of the profile (< 1 %RH), but is up to ± 3 %RH in the most sensitive locations where the measured humidity gradient changes relatively abruptly at cold temperatures.

d. Incorporation of bias corrections

Corrections for the TD and contamination errors for RS80 radiosondes should be performed first, then the time-lag correction is applied to the bias-corrected profile. Although the bias corrections are simply equations that depend on the measured temperature and humidity, they cannot be applied to the original measurements before the skeleton profile is defined, because the skeleton definition is based on integer constant-RH periods. The skeleton profile and smoothing tolerance are first established from the original data, then the bias corrections are calculated and added to each skeleton point, then the smoothing operations and time-lag correction are performed on the bias-corrected profile.

Figure 6f shows the example profile after first correcting the TD error (green), and then correcting for time-lag error (red). Since this radiosonde was produced after 1 June 2000, the contamination correction is zero. Ice-saturation at the tropopause (-73°C) is 49 %RH, suggesting this is a tropopause cirrus layer approximately 1 km thick (within a few %RH absolute

accuracy), which would not be apparent from either the original measurements or the bias-corrected measurements.

e. Important algorithm details

The correction approach described in Section 3c applies to standard Vaisala data with 1 %RH resolution, and the approach must be modified for higher-resolution data (e.g., 0.1 %RH). In these cases, it is not necessary to construct a skeleton profile before applying the smoothing *if* the sample spacing is greater than about 6 s, as demonstrated in Section 4. If the sample spacing for 0.1 %RH data is less than about 6 s, inherent “noise” from the instrumentation and raw data processing leads to noisy results, because the critical ratio $\Delta t/\tau$ becomes strongly influenced by the noise. One approach in these cases is to degrade the resolution of the data to 1 %RH by rounding to the nearest integer, then proceed with the standard correction procedure described in Section 3c; however, information on the fine-scale vertical structure in the humidity profile will be lost. The recommended approach is to use the full resolution of the data and instead degrade the sample spacing to at least 6 s by averaging then subsampling.

Instrument noise must be removed prior to performing the time-lag correction. A useful temperature-dependent criterion for identifying “spikes” in the data is to limit the *ambient* (corrected) humidity gradient to a maximum of 12 %RH s⁻¹, which corresponds to the condition $dU_m/dt < 12 \cdot (1 - e^{-1/\tau})$, where the latter factor is the fractional sensor response in 1 s. Single-point peaks in the original data (e.g., at 11.5 km altitude in Fig. 6) are artifacts of the low resolution and raw data processing. These are set equal to the previous value, and wider peaks at cold temperatures are treated similarly if their duration is less than 0.1τ . Throughout the correction algorithm, threshold values and adjustable parameters are specified in terms of slopes or the time-constant, which generalizes the algorithm for different sensor types and timesteps.

4. Evaluation of the Correction Algorithm

Corrections for time-lag, TD, and contamination errors were applied to a dataset of 40 simultaneous soundings from RS80-H radiosondes and the NOAA/CMDL cryogenic frostpoint

hygrometer, conducted monthly between July 1998 and March 2002 at Boulder, Colorado. The NOAA hygrometer is a relatively fast-response instrument with a known measurement uncertainty (Vömel et al. 1995; Oltmans and Hofmann 1995; M01). The hygrometer is used in this study as a reference instrument for evaluating the radiosonde measurements and corrections. All soundings were conducted during the daytime, so possible day/night differences and solar radiation effects cannot be evaluated with this dataset.

a. The NOAA/CMDL cryogenic hygrometer

The hygrometer measures water vapor concentration based on the chilled-mirror principle, where the temperature of a mirror is controlled to maintain a constant thin layer of frost coverage, and this equilibrium temperature is the frostpoint temperature of the air (T_f). The mirror can be heated electrically or rapidly cooled by a cryogenic liquid. The relative humidity is calculated from T_f and from the air temperature (T) measured by the radiosonde, according to: $RH = e_i(T_f)/e_w(T) \times 100\%$, where e_i is the saturation vapor pressure over ice as given by Hyland and Wexler (1983):

$$\ln(e_i) = A \cdot \ln(T) + \sum_{i=0}^5 a_i \cdot T^{i-1}, \quad (5)$$

where T (or T_f) is in degrees K, e_i is in dyne cm^{-2} , $A=4.1635019$, $a_0=-5.6745359\text{e}3$, $a_1=6.3925247$, $a_2=-9.6778430\text{e}-3$, $a_3=6.2215701\text{e}-7$, $a_4=2.0747825\text{e}-9$, and $a_5=-9.4840240\text{e}-13$; and e_w is the saturation vapor pressure over water as given by Wexler (1976):

$$\ln(e_w) = B \cdot \ln(T) + \sum_{i=0}^6 b_i \cdot T^{i-2}, \quad (6)$$

where $B=2.858487$, $b_0=-2.9912729\text{e}3$, $b_1=-6.0170128\text{e}3$, $b_2=1.887643854\text{e}1$, $b_3=-2.8354721\text{e}-2$, $b_4=1.7838301\text{e}-5$, $b_5=-8.4150417\text{e}-10$, and $b_6=4.4412543\text{e}-13$. These particular saturation vapor pressure formulations are used in part because Vaisala's TD calibration equations were

determined using these formulations. Discussion of different saturation vapor pressure formulations can be found in Appendix B of M01.

The fractional uncertainty in RH calculated from the hygrometer measurements, given by estimated uncertainties of $\pm 0.5^\circ\text{C}$ in both T_f and T , varies with temperature from 0.06 at 0°C to 0.10 at -70°C (e.g., the uncertainty in a calculated RH value of 30 %RH at -70°C is ± 3 %RH). This constitutes the accuracy limit for which comparisons between the radiosonde and hygrometer data are meaningful. It should be noted that the Vaisala “ground check correction” was not applied to the NOAA RS80-H data. The GC correction is intended to remove the calibration bias for individual radiosondes using a prelaunch radiosonde measurement at 0% ambient RH, determined by placing the sensor in a chamber containing desiccant. However, W02 give several reasons to avoid the GC correction, especially for radiosondes whose bias is partly due to contamination.

b. Algorithm validation

The NOAA data are output with a resolution of 0.1 %RH and a sample spacing of 8 s, so these data are not characterized by the “stairsteps” of 1 %RH resolution data as described in Section 3c and Fig. 6. The corrections and smoothing operations are therefore applied directly to the original RS80-H data without constructing a skeleton profile, as described in Section 3e. Almost all of the radiosondes were produced before June 2000, so they are corrected for contamination error as well as time-lag and TD error.

Four of the 40 RS80-H/hygrometer soundings are shown in Fig. 7, illustrating two main conclusions about the performance of the correction algorithm (compare red vs purple curves). First, the time-lag correction is seen to recover vertical structure in the radiosonde profile that had been “smoothed” by slow sensor response at low temperatures. Much more vertical structure exists in humidity profiles in the UT than is apparent from the original radiosonde data, but the “information” about the vertical structure is present in the measured humidity gradient. The general accuracy of the laboratory time-constant measurements and their validity under

operational conditions are also verified by Fig. 7 (as well as by the other 36 profiles, which are generally similar).

The second main conclusion from Fig. 7 is that there is a residual bias in the corrected radiosonde data relative to the hygrometer. The magnitude of the residual bias is not a function of the temperature but appears to depend on the radiosonde age, where “young” radiosondes are undercorrected (Fig. 7c), and “old” radiosondes are overcorrected (Fig. 7d). One cause of the residual bias is found in the age-dependent factor of the contamination correction, which is shown in Appendix C to suffer from two shortcomings: an erroneous polynomial fit for radiosonde ages greater than about 3 years (Fig. C1); and an insufficient dataset for meaningful assessment of the contamination process outside the age range 0.5-3 years. Analysis presented below and in Appendix C supports the conclusion that contamination occurs rapidly and reaches a constant “saturation” level by about age 1 year. As justified in Appendix C, we recommend that all RS80-H radiosondes produced before June 2000, regardless of age, be treated as if they are 1 year old when calculating the contamination correction from Eq. (4.1-H) in W02. This “modified contamination correction” is used throughout the remainder of this paper.

The profile-average bias between each RS80-H and hygrometer profile is shown as a function of the radiosonde age in Fig. 8, where the bias was calculated for only altitudes below the tropopause and temperatures below -15°C (at higher temperatures there is ambiguity as to whether the hygrometer is measuring the frostpoint or the dewpoint). Before applying any corrections (Fig. 8a), the mean dry bias for the dataset as a whole is $-6.4\% \text{RH}$, and the range of variability at any given age is about $\pm 6\% \text{RH}$. The mean and variability are both on average independent of the radiosonde age as judged by the best-fit curve. Figure 8b shows the mean residual bias of each sounding after correcting for time-lag, TD, and contamination errors using the contamination correction as given by W02 (but limited to a maximum age of 4 years due to the erroneous polynomial fit, as was also done in Fig. 7d). The tendency suggested by Fig. 7 for the W02 contamination correction to undercorrect young radiosondes and overcorrect old radiosondes is seen to be true in general for the NOAA dataset. The modified contamination correction from Appendix C eliminates the residual mean bias on average for all radiosondes except those younger than 1 year, which remain drier than the hygrometer by about $4\% \text{RH}$ on

average (Fig. 8c). The range of variability at a given age has also been reduced somewhat by the corrections to about ± 4 %RH. The humidity-dependent factor in the W02 contamination correction appears to be reasonable and consistent with the NOAA data, as there is no substantial difference in the corrected results between generally drier soundings (open circles) and generally moister soundings (filled circles). Residual variability is attributed to three general causes: 1) variability in the contamination process relative to the mean contamination correction, which may vary substantially between batches that have experienced different temperatures during shipping and storage; 2) variability in the accuracy of the Vaisala calibration (Turner et al. 2003), which consists of both a random component given by the accuracy of the polynomial calibration models for a given individual sensor (“production variability”), and a bias component that varies between calibration batches and may represent the absolute accuracy of the Vaisala calibration procedure; and 3) uncertainty in the hygrometer measurements, which is random for a large dataset, but is a bias for any individual sounding.

The temperature-dependence of the RS80-H/hygrometer comparison is shown in Fig. 9. The mean dry bias in the original RS80-H data relative to the hygrometer (Fig. 9a) increases with decreasing temperature from about -4 %RH at -20°C to about -12 %RH at -70°C , with substantial variability about the mean especially at low temperatures, as judged by the 68th percentile curves (which are analogous to the standard deviation but are more appropriate for an asymmetric distribution). After applying the time-lag, TD, and modified contamination corrections (Fig. 9c), the mean bias is reduced to about ± 2 %RH at all temperatures, and the variability is reduced substantially, especially at low temperatures, due in part to recovery of vertical structure in the profile by the time-lag correction. Note that when the original contamination correction is used (Fig. 9b), variability actually increases over much of the temperature range due to the age-dependence of the residual bias.

In summary, Fig. 7 demonstrates that the time-lag correction substantially improves the accuracy of Vaisala radiosonde humidity measurements by recovering vertical structure in the humidity profile, especially in the UT and tropopause region. Figures 8 and 9 demonstrate that the combination of time-lag, TD, and the modified contamination correction largely eliminates the temperature-dependent mean bias in the uncorrected data, and reduces the variability. The

contamination correction, while certainly reducing the bias error on average, remains the largest source of uncertainty in individual corrected profiles for radiosondes produced before June 2000.

RS80 radiosondes produced after 1 June 2000 are shipped with a sealed sensor cap that protects the sensor from chemical contamination, so the corrected data will not contain the associated large uncertainty. Ferrare et al. (2004) compared post-contamination RS80-H measurements with coincident water vapor measurements from the airborne LASE (Lidar Atmospheric Sensing Experiment) during the ARM-FIRE Water Vapor Experiment (AFWEX) in December 2000 at the Oklahoma ARM site. LASE is an airborne DIAL (Differential Absorption Lidar) that measures water vapor profiles with an established absolute accuracy of better than 6% (percentage, not %RH). The study showed that the time-lag and TD corrections decreased the mean dry bias of the radiosonde measurements relative to LASE in the uppermost 4 km of the troposphere from >15% to <5%. Similar agreement between LASE and the corrected radiosonde data ($\pm 5\%$) was found throughout the troposphere. Comparisons between LASE and a ground-based Raman lidar near the radiosonde launch site were within $\pm 4\%$ throughout the troposphere, giving additional confidence in the accuracy of the corrected radiosonde measurements, and the success of the sealed sensor cap in reducing or eliminating the contamination error.

c. Ice-supersaturation and supercooled liquid water

The NOAA hygrometer is inherently capable of measuring ice-supersaturation, which provides a means of evaluating RS80-H measurements under these conditions. Ice-supersaturation cannot readily be generated in a calibration chamber, so the accuracy of the sensor calibration under these conditions has never been evaluated in the laboratory. It seems plausible that a layer of ice might deposit on the sensor surface and limit the humidity of the air that reaches the sensor polymer to ice-saturation.

The corrected RS80-H measurements in the ice-supersaturated region in Fig. 7b are in quantitative agreement with the hygrometer and show the same vertical structure, suggesting that Vaisala humidity sensors are indeed capable of measuring ice-supersaturation. Figure 10 shows

the difference between corresponding RS80-H and hygrometer datapoints before and after correction, as in Fig. 9, but for only those instances when the hygrometer measured ice-supersaturation. Although the dataset is too small to make rigorous quantitative statements, the corrections clearly improve the accuracy of the radiosonde data substantially, indicating that the sensor responds roughly the same to conditions above ice-saturation as to conditions below ice-saturation. This conclusion is consistent with the manufacturer's assertion (M01) that water vapor is absorbed into the structure of the sensor polymer as individual molecules rather than as clusters of molecules, where clustered molecules can freeze in lower-quality sensor polymers.

A phenomenon called “sensor icing” occurs when RS80 radiosondes pass through supercooled liquid water and the sensor becomes wet and freezes at temperatures below 0°C. A coating of ice forms on the sensor and causes the measurement to remain near ice-saturation at altitudes above the icing event, even into the stratosphere (Fig. 11). Sensor icing can also occur below water saturation in thick ice clouds. It is important that users of RS80 data inspect the data for potential sensor icing, and disregard measurements above the icing level. The RS90 and RS92 radiosondes, in addition to improved calibration accuracy and faster sensor response, eliminate sensor icing by using dual humidity sensors that are alternately heated to remove ice while the other sensor makes the measurement (Paukkunen 1995).

5. Impact of the Corrections

The magnitude of the humidity correction depends on the radiosonde type and on the particular humidity and temperature profiles measured. The Vaisala radiosonde types differ substantially in the accuracy of their TD calibrations and their time-response, and the accuracy of the two RS80 radiosonde types depends on whether or not they are affected by contamination. Since the TD correction is proportional to temperature and humidity, and the time-lag correction depends on temperature and the local humidity gradient, the magnitude of the correction will vary with both geographic location (e.g., mid-latitude vs tropics), and with the season at a given location. This section evaluates the dependence of the correction on location and season, using Intensive Observing Period (IOP) datasets from the DOE/ARM site in northern Oklahoma, and

from south Florida sites during CRYSTAL-FACE (Cirrus Regional Study of Tropical Anvils and Cirrus Layers – Florida Area Cirrus Experiment) in July 2002.

a. Radiosondes produced after 1 June 2000

The contamination correction is not applied to radiosondes produced after 1 June 2000. The close agreement during AFWEX between LASE and RS80-H measurements corrected for time-lag and TD errors (Ferrare et al. 2004) gives confidence that the contamination has at least been substantially reduced by the sealed sensor cap. Figure 12 shows the amount of correction as a function of altitude for all soundings acquired during AFWEX. The mean and standard deviation of the correction in 1 km altitude increments is shown in the top panels in terms of %RH, and in the bottom panels as a percentage of the measured RH. The total correction (time-lag + TD) is shown in the left panels, and the separate contributions from the TD or time-lag correction alone are shown in the center and right panels. The following conclusions can be drawn from Fig. 12:

- The correction is essentially zero in the lower troposphere, because the TD correction is negligible and the sensor time-response is relatively fast at temperatures above about -30°C .
- The total correction (left panels) increases the mean water vapor concentration in the UT by up to 4 %RH (or 13% in absolute terms), and decreases the mean water vapor concentration in the LS by up to -4 %RH (or -35%, which is a large percentage because the stratospheric humidity is very low). The variability between soundings is large, and the correction for some soundings exceeds 25% in the UT and -55% in the LS.
- The contribution from the TD correction (center panels) reflects the mean humidity and temperature profiles during AFWEX, and their variability. The peak in the TD correction is at the tropopause (panel b), because the temperature is lowest and the mean humidity is relatively high compared to the LS. The percentage TD correction remains about 15% in the stratosphere (panel e), but it is 15% of the very low stratospheric RH and is not particularly meaningful.

- The contribution from the time-lag correction (right panels) mainly reflects the temperature profile and the local humidity gradient, where the latter can vary substantially at a given altitude and accounts for the large variability between soundings. The time-lag correction can be either positive or negative, and a contribution of the time-lag correction to the mean implies that the humidity at a given altitude is preferentially either increasing or decreasing. The mean time-lag correction reflects the common occurrence of increasing RH below a high humidity layer near the tropopause, followed by decreasing RH above the tropopause into the LS. One consequence of this common atmospheric structure is that the time-lag correction steepens the humidity gradient and narrows the thickness of the troposphere-stratosphere transition region.

The correction for a given sounding depends on the structure of the humidity and temperature profiles, as well as the radiosonde sensor type. Figure 13 shows the percentage correction as a function of altitude for soundings from two south Florida sites during CRYSTAL-FACE, in comparison to the AFWEX dataset. The Miami NWS site used RS80-H radiosondes (panel a), and the Everglades City site used RS90 radiosondes from the PNNL (Pacific Northwest National Laboratory) mobile facility (panel b). The Miami and AFWEX datasets (both RS80-H) show the same general characteristics that the corrections increased the water vapor in the UT, decreased the water vapor in the LS, and exhibit large variability between soundings due to the time-lag correction. The greater mean water vapor increase in the UT of 21% for Miami (versus 13% for AFWEX) mostly reflects the higher tropopause altitude, colder temperatures in the UT, and higher mean humidity at the Miami site. Results from the Tampa NWS site (not shown) are almost identical to the Miami results. The RS90 dataset (panel b), which sampled synoptic conditions that were generally similar to the Miami site, shows only a small increase in UT water vapor and considerably less variability than the RS80-H datasets, due to the faster sensor time-response and absence of a TD correction. The mean water vapor in the LS is still reduced by 20% due to the consistent negative humidity gradient above the tropopause.

These examples illustrate the important point that comparisons of *uncorrected* radiosonde data between different sites (or between seasons at the same site) actually reflect the sum of real differences in the atmospheric profiles plus differences in the measurement error that are a

function of the real differences. That is, climatologies contain variability that in part results from variability in the measurement error.

b. Radiosondes produced before 1 June 2000

In addition to the time-lag and TD corrections, Vaisala RS80 radiosondes manufactured before June 2000 should be corrected for chemical contamination error using the modified contamination correction described in Appendix C. Figure 14 shows the percentage correction for several ARM IOP datasets that used RS80-H radiosondes produced before June 2000. Whereas the AFWEX results (Fig. 12d) show that the time-lag and TD corrections are essentially zero in the lower troposphere, the contamination correction for these datasets is 10-20% in the lower troposphere, where most of the total-column PW resides. The correction increases with altitude to a mean of 50-100% at the tropopause, with substantial variability between soundings. The large uncertainty in the contamination correction seriously limits the accuracy of any individual corrected sounding.

6. Conclusions

This study has concerned improving the accuracy of Vaisala radiosonde humidity measurements, especially in the UT, by applying sensor-based corrections for well-understood sources of measurement error. Laboratory measurements of the sensor time-constant conducted by Vaisala were used to develop a correction for time-lag error that is caused by slow sensor response at cold temperatures. RS80 radiosondes were also corrected for temperature-dependence (TD) error that results from inaccuracy in the sensor calibration at cold temperatures, and RS80 radiosondes produced before June 2000 were corrected for chemical contamination error that is caused by the occupation of binding sites in the sensor polymer by non-water molecules outgassed from the radiosonde packaging material.

The correction algorithm was evaluated by comparing corrected RS80-H measurements with simultaneous measurements from the reference-quality NOAA/CMDL cryogenic hygrometer. The time-lag correction recovers vertical structure in the humidity profile that had been highly

smoothed by slow sensor response at cold temperatures (Fig. 7). The time-lag correction, on average, increases water vapor in the UT, decreases water vapor in the LS, and reveals a much sharper troposphere-stratosphere transition than is indicated by the original measurements. The sensitivity of the time-lag correction to the local humidity gradient leads to considerable variability between soundings in the sign and magnitude of the correction at a given altitude. The time-lag correction procedure requires a smooth time-series of humidity measurements, and a new derivative-based numerical technique was developed to smooth time-series data within a specified tolerance, thereby preserving consistency with the original data at all scales.

Statistical analysis of the difference between corresponding RS80-H and NOAA hygrometer measurements (Fig. 9) shows that the corrections reduced the mean radiosonde dry bias from 4 %RH at -20°C and 10 %RH at -70°C to about ± 2 %RH at all temperatures. Variability in the RS80-H/hygrometer comparison was reduced by the time-lag correction, and residual variability is due in part to large uncertainty in the statistical contamination correction for any individual sounding. An age-dependent residual bias (Fig. 8) revealed shortcomings in the contamination correction as given by W02 (Fig. C1), and we recommend specifying a constant radiosonde age of 1 year when calculating the contamination correction. It was also shown that Vaisala humidity sensors are capable of measuring ice-supersaturation, and that RS80 sensors are susceptible to sensor icing.

The corrections were applied to several IOP datasets, including RS90 radiosondes and RS80-H radiosondes produced both before and after June 2000. The mean percentage correction in the UT for RS80-H radiosondes produced after June 2000 (time-lag and TD corrections) varies with geographic location and season, and was 13% for Oklahoma wintertime soundings (AFWEX) and 20% for south Florida summertime soundings (CRYSTAL-FACE). The mean percentage correction in the UT for RS80-H radiosondes produced before June 2000 (time-lag, TD, and contamination corrections) during several ARM IOPs was about 10% at the surface and increased with decreasing temperature to 50-100% at the tropopause. The mean percentage correction for RS90 radiosondes in the UT during CRYSTAL-FACE was <5% (time-lag correction only).

Acknowledgements

The authors are grateful to June Wang and Hal Cole (NCAR/ATD) and Barry Lesht (ANL) for numerous enlightening discussions about Vaisala radiosondes. We thank David Starr and Andrew Lare (NASA/GSFC), and Jim Mather and the crew of the PNNL PARSL facility, for their effort in acquiring the radiosonde data during the NASA/CRYSTAL-FACE experiment. This work was primarily supported by the Biological and Environmental Research Program (BER), U.S. Department of Energy, Grant Nos. DE-FG03-00ER62929 and DE-FG03-02ER63317. Additional support was received from the NASA/CRYSTAL-FACE program, Reference No. 10-06924.

Appendix A --- Vaisala Radiosonde Serial Numbers

The “age” of a radiosonde is defined as the time between the factory calibration and the launch. The calibration date is encoded in the radiosonde serial number, with separate encoding schemes for RS80 and RS90 radiosondes. Furthermore, the RS80 scheme was changed in October 1995. There are 9 characters in RS80 serial numbers, and 8 characters in RS90 serial numbers. The RS80-H cannot be distinguished from the RS80-A based solely on the serial number. See M01 (Appendix A) for advice on distinguishing the two RS80 models. The beginning portion of the serial number encodes the calibration date as shown below, where ‘x’ is just a sequence number.

- RS80 A/H radiosondes calibrated prior to October 1995: code = DDMMYxxxx
DD = day of month (01-31)
MM = month (01-12) + facility identifier (00, 20, 40, or 80)
Y = last digit of year
- RS80 A/H radiosondes calibrated October 1995 or later: code = YWWDxxxxx
Y = last digit of year
WW = week number (01-52)
D = day of week (1-7, Monday=1)

- RS90/RS92 radiosondes: code = YWWDxxxx
 Y = alphabetic code for year (T=1998, U=1999, etc.)
 WW = week number (01-52)
 D = day of week (1-7, Monday=1)

Appendix B --- Derivative-Based Smoothing Algorithm

The time-lag correction is very sensitive to changes in the slope of the humidity profile at low temperatures, which requires some means of smoothing the data while still maintaining consistency with the original data at all scales. This appendix describes the numerical implementation of an algorithm that produces a locally smooth time-series by minimizing the third derivative of the data subject to specified constraints on the amount that any datapoint may move. The algorithm attempts to maintain constant curvature to the extent that is possible within the specified smoothing tolerance. This smoothing technique has advantages over other approaches such as averaging, polynomial smoothing, and Fourier or wavelet techniques, in situations when only local smoothness is required. The flexibility to specify tolerances for each data point preserves features in the data at all scales, and the sample spacing can be irregular since this approach is based on slopes. Figure B1 illustrates the algorithm performance for various values of the smoothing tolerance parameter Δy and independent variable t .

The mathematically-astute reader will immediately note that this problem has no unique solution, as any adjustment that improves the smoothness at point i may reduce the smoothness at point $i+1$. The smoothing algorithm is iterative and seeks a balance between the competing interests of neighboring points. Notation such as the following will be used in this discussion: $D_3[i+2]$ refers to the third back-derivative of y calculated at point $i+2$, in which case $D_3[i+2] = (D_2[i+2] - D_2[i+1]) / \Delta t[i+2]$, where $\Delta t[i+2] = t[i+2] - t[i+1]$. The upper and lower limits of the smoothing tolerance range for point i are designated as $y_H[i]$ and $y_L[i]$ respectively, where nominally $y_H[i]=y[i]+\Delta y[i]$ and $y_L[i]=y[i]-\Delta y[i]$, although the tolerance range does not need to be symmetric about $y[i]$. The new (smoothed) value of $y[i]$ is designated $y_s[i]$.

Proceeding through the array y in the forward direction and ignoring endpoints for the moment, if the smoothed value $y_s[i]$ has been determined, then $y_s[i+1]$ will be the value within the range $y_L[i+1]$ to $y_H[i+1]$ that minimizes $D_3[i+2]$. For the first iteration, $D_3[i+2]$ is calculated from the original (unsmoothed) value $y[i+2]$, but for subsequent iterations the value $y_s[i+2]$ from the previous iteration is used. In the original (and highly inefficient) implementation of this algorithm, $D_3[i+2]$ was calculated for 100 evenly-spaced choices of $y_s[i+1]$ between its tolerance limits, and the chosen $y_s[i+1]$ value was that which minimized $|D_3[i+2]|$. However, a more efficient and accurate approach was recognized that involves first calculating the critical constant-curvature value, $y_c[i+1]$, that yields $D_3[i+2]=0$. The condition $D_3[i+2]=0$ means that $D_2[i+2]=D_2[i+1]$, where the appropriate substitutions and some algebra lead to the constant-curvature value $y_c[i+1]$:

$$y_c[i+1] = \frac{(D_1[i] \cdot \Delta t[i+2]^2) + (y[i+2] \cdot \Delta t[i+1]) + (y[i] \cdot \Delta t_{fac})}{\Delta t[i+1] + \Delta t_{fac}}, \quad (\text{B1})$$

where $\Delta t_{fac} = (\Delta t[i+2]/\Delta t[i+1]) \cdot (\Delta t[i+2] + \Delta t[i+1])$. If $y_c[i+1]$ is within the smoothing tolerance range then it is accepted as the new smoothed value, $y_s[i+1] = y_c[i+1]$. If $y_c[i+1] > y_H[i+1]$, then the minimum acceptable $|D_3[i+2]|$ must occur when $y_s[i+1] = y_H[i+1]$. Similarly, if $y_c[i+1] < y_L[i+1]$, then the minimum acceptable $|D_3[i+2]|$ must occur when $y_s[i+1] = y_L[i+1]$.

The above procedure is biased toward smoothing the data as viewed in the “forward” direction, but the “reverse” direction is equally valid and generally leads to a different result. A compromise is achieved by also computing the smoothed array in the reverse direction, then accepting the average of the forward and reverse results at each point as the smoothed array, y_s . The process is then repeated, where the fixed “aiming point” is now $y_s[i+2]$ from the previous iteration. Usually the solution changes very little after three iterations. The two points at each end of the array are treated separately after each iteration. The minimum D_3 for the next-to-the-endpoint is calculated for each of 100 equally-spaced points in the endpoint tolerance range, and the pair of points that minimizes $|D_3|$ are chosen. Often several pairs produce $D_3=0$, so a second

criterion is used to select the optimal pair. One possibility is to choose the pair that has the minimum $|D_2|$ (i.e., closest to linear at the ends).

A second algorithm is needed to smooth *corrected* humidity profiles, while constraining the amount by which the *measured* profile is smoothed. Due to the complicated relationship between the corrected and measured points via Eqs. (3) and (4), a desired smoothing tolerance for the measured points might allow a much larger amount of smoothing for the corrected points, especially at cold temperatures where the correction is very sensitive to the slope of the measured profile. The goal of this second algorithm is to maximize the amount of smoothing of the corrected profile while ensuring that no measured point is moved more than the specified smoothing tolerance when the corresponding measured profile is calculated from Eq. (3). This is accomplished by first applying the smoothing algorithm to the corrected profile with an initial guess for the smoothing tolerance, then calculating the corresponding measured profile from Eq. (3) and evaluating the impact on the measured profile to either expand or restrict the smoothing tolerance for certain points in the corrected profile for subsequent iterations. If a given measured point is outside its specified range, then the responsible corrected point(s) must be restricted for the next iteration. Conversely, if a given corrected point is at the limit of its smoothing tolerance but more allowable smoothing is available for the corresponding measured point, then the smoothing tolerance for the corrected point can be expanded for the next iteration. Since a change to any given point can affect subsequent points, it is necessary to evaluate whether expansion of the smoothing range for a given corrected point might cause subsequent measured points to be thrown out of their smoothing tolerance range in the next iteration. There is a certain amount of unpredictability in this system, so conservative changes are merited. It is helpful to predict the effect of moving one point on subsequent points, and this can be accomplished using derivatives of the discrete forms of Eqs. (3) and (4).

Appendix C --- Modified RS80-H Contamination Correction

The RS80-H contamination correction given by W02 (Fig. 1d) exhibits a suspicious age-dependence, where the contamination at a given RH increases with time up to age 1 year, then is nearly constant for years 1-3, but then increases dramatically for radiosondes older than 3 years.

In contrast, the RS80-A contamination rate slows with increasing age (Fig. 1c), asymptotically approaching a constant “saturation” value, as intuition might suggest if the contamination rate is viewed as being proportional to the number of susceptible binding sites that are not yet contaminated. The RS80-H contamination correction is instead plotted as a function of the radiosonde age in Fig. C1, where vertical lines indicate the five radiosonde ages that were used to derive the correction (from W02, Table 2), and asterisks indicate the ages of the NOAA radiosondes. Clearly the peak at age 5 years and subsequent *decrease* in contamination for older radiosondes are erroneous artifacts of the polynomial fitting. The age used to compute the contamination correction for the 6.7 year old radiosonde shown in Fig. 7d was arbitrarily set to 4 years for demonstration purposes, because the calculated contamination correction was actually negative. The correction for RS80-H radiosondes younger than 0.5 years is also in question because there were no data to distinguish whether the contamination process is gradual (as is assumed by specifying zero correction at zero age), or whether the contamination process occurs rapidly and reaches a “saturation” amount (as suggested by the constancy of the correction in the age range 1-3 years). The single datapoint at age 5.5 years does suggest that contamination may again increase after age 3 years, but this behavior seems implausible and is likely the result of large variability in contamination and the limited sample size of 4 radiosondes (these radiosondes may be more contaminated than average because they were exposed to high storage temperatures in the tropics during TOGA COARE).

The mean bias between the hygrometer and uncorrected RS80-H profiles (Fig. 8a) displays considerable variability between soundings (± 6 %RH), and on average is independent of the radiosonde age, suggesting that these radiosondes were “fully contaminated” prior to launch regardless of the radiosonde age. Both the NOAA dataset and the W02 dataset suggest that RS80-H radiosondes are fully contaminated by age 1 year, and therefore all radiosondes of age one year or older should be treated as if they are one year old when calculating the contamination correction. [Note that it makes little difference which age in the range 1-2.5 years is used to represent full contamination, since the polynomial fit is constant throughout this range.] Correction of the NOAA dataset using a constant age of 1 year for the contamination correction (Fig. 8c) shows that both the NOAA and the W02 datasets are consistent with the notion that radiosondes older than 1 year are fully contaminated.

Interpretation of the contamination bias for radiosondes younger than one year is less clear. The W02 data at the single age of 0.46 years shows that on average these 7 radiosondes are contaminated by approximately 70% of the saturation value, whereas the NOAA data show that the contamination in the age range 0.1-0.7 years actually *exceeds* the saturation value since a residual mean dry bias remains after the data are corrected assuming a radiosonde age of 1 year (Fig. 8c). Since contamination is produced by outgassing of volatiles from the radiosonde packaging material, it is a temperature-dependent process, and both the time required to reach full contamination and the amount of contamination when saturated may vary considerably depending on the temperatures experienced by the radiosondes during transport and storage. According to this view, the young NOAA radiosondes must have experienced higher temperatures than the young W02 radiosondes, leading to both more rapid contamination and a higher level of saturated contamination. However, Turner et al. (2003) found that the accuracy of the Vaisala calibration varied between calibration batches, which could contribute to either the apparent undercorrection of the young NOAA radiosondes in Fig. 8c, or the W02 estimate of contamination at age 0.46 years. Variability due to calibration accuracy can't be distinguished from variability in the contamination process.

The NOAA and W02 datasets both clearly support the conclusion that contamination reaches a saturation level by age 1 year, and therefore all radiosondes older than one year should be treated as if they are 1 year old when calculating the correction. There is considerable variability in the residual bias between radiosondes of the same age (± 4 %RH is suggested by Fig. 8c). There is additional uncertainty for radiosondes younger than one year due in part to the poorly known time required to reach saturated contamination and its dependence on storage temperature. This study has assumed that *all* radiosondes are saturated with contamination regardless of their age (as supported by Fig. 8), and therefore a constant age of 1 year was used to calculate the contamination correction from W02.

REFERENCES

Blackmore, W.H., and B. Taubvurtzel, 1999: Environmental chamber tests of NWS radiosonde relative humidity sensors. Preprints, *11th Symp. on Meteorological Observations and Instrumentation*, Dallas, Texas, Amer. Meteor. Soc., 259-262.

Elliott, W.P., R.J. Ross, and W.H. Blackmore, 2002: Recent changes in NWS upper-air observations with emphasis on changes from VIZ to Vaisala radiosondes. *Bull. Amer. Meteor. Soc.*, **83**, 1003-1017.

Elliott, W.P., and D.J. Gaffen, 1991: On the utility of radiosonde humidity archives for climate studies. *Bull. Amer. Meteor. Soc.*, **72**, 1507-1520.

Ferrare, R.A., E.V. Browell, S. Ismail, S. Kooi, L.H. Brasseur, V.G. Brackett, M. Clayton, J. Barrick, G. Diskin, J. Goldsmith, B. Lesht, J. Podolske, G. Sachse, F.J. Schmidlin, D. Turner, D. Whiteman, D. Tobin, L. Miloshevich, 2004: Characterization of upper troposphere water vapor measurements during AFWEX using LASE. *J. Atmos. Oceanic Technol.* Submitted.

Ferrare, R.A., S.H. Melfi, D.N. Whiteman, K.D. Evans, F.J. Schmidlin, and D.O'C. Starr, 1995, a comparison of water vapor measurements made by Raman lidar and radiosondes. *J. Atmos. Oceanic Technol.*, **12**, 1177-1195.

Heymsfield, A.J. and L.M. Miloshevich, 1995: Relative humidity and temperature influences on cirrus formation and evolution: Observations from wave clouds and FIRE-II. *J. Atmos. Sci.*, **52**, 4302-4326.

Hirvensalo, J., J. Wahn, and H. Jauhiainen, 2002: New Vaisala RS92 GPS radiosonde offers high level of performance and GPS wind data availability. Preprints, *12th Symp. on Meteorological Observations and Instrumentation*, Long Beach, California, Amer. Meteor. Soc., 4-9.

Hyland, R.W., and A. Wexler, 1983: Formulations for the thermodynamic properties of the saturated phases of H₂O from 173.15 K to 473.15 K. *ASHRAE Transactions*, Part 2A. pp 500-519.

Lorenc, A.C., D. Barker, R.S. Bell, B. Macpherson, and A.J. Maycock, 1996: On the use of radiosonde humidity observations in mid-latitude NWP. *Meteor. Atmos. Phys.*, **60**, 3-17.

Miloshevich, L.M., H. Vömel, A. Paukkunen, A.J. Heymsfield, and S.J. Oltmans, 2001: Characterization and correction of relative humidity measurements from Vaisala RS80-A radiosondes at cold temperatures. *J. Atmos. Oceanic Technol.*, **18**, 135-156.

Oltmans, S.J., and D.J. Hofmann, 1995: Increase in lower stratospheric water vapour at a mid-latitude Northern Hemisphere site from 1981 to 1994. *Nature*, **374**, 146-149.

Paukkunen, A., V. Antikainen, and H. Jauhiainen, 2001: Accuracy and performance of the new Vaisala RS90 radiosonde in operational use. *11th AMS Symposium on Meteorological Observations and Instrumentation*, Albuquerque, New Mexico, 14-18 January, 98-103.

Paukkunen, A., 1995: Sensor heating to enhance reliability of radiosonde humidity measurement. *11th AMS International Conference on Interactive Information and Processing Systems for Meteorology, Oceanography, and Hydrology*, Dallas, Texas, 15-20 January, 103-106.

Revercomb, H.E., D.D. Turner, D.C. Tobin, R.O. Knuteson, W.F. Feltz, J. Barnard, J. Bosenberg, S. Clough, D. Cook, R. Ferrare, J. Goldsmith, S. Gutman, R. Halthore, B. Lesht, J. Liljegren, H. Linne, J. Michalsky, V. Morris, W. Porch, S. Richardson, B. Schmid, M. Splitt, T. Van Hove, E. Westwater, and D. Whiteman, 2003: The ARM program's water vapor intensive observation periods: Overview, initial accomplishments, and future challenges. *Bull. Amer. Meteor. Soc.*, **84**, 217.

Ross, R.J. and D.J. Gaffen, 1998: Comment on "Widespread tropical atmospheric drying from 1979 to 1995" by Schroeder and McGuirk. *Geophys. Res. Lett.*, **25**, 4357-4358.

Schroeder, S.R. and J.P. McGuirk, 1998: Widespread tropical atmospheric drying from 1979 to 1995. *Geophys. Res. Lett.*, **25**, 1301-1304.

Soden, B.M. and J.R. Lanzante, 1996: An assessment of satellite and radiosonde climatologies of upper-tropospheric water vapor. *J. Climate*, **9**, 1235-1250.

Soden, B.J., D.D. Turner, B.M. Lesht, and L.M. Miloshevich, 2004: An analysis of satellite, radiosonde, and lidar observations of upper tropospheric water vapor from the ARM program. *J. Geophys. Res.* Accepted.

Turner, D.D., B.M. Lesht, S.A. Clough, J.C. Liljegren, H.E. Revercomb, and D.C. Tobin, 2003: Dry bias and variability in Vaisala RS80-H radiosondes: The ARM experience. *J. Atmos. Oceanic Technol.*, **20**, 117-132.

Vömel, H., S.J. Oltmans, D.J. Hofmann, T. Deshler, and J.M. Rosen, 1995: The evolution of the dehydration in the Antarctic stratospheric vortex. *J. Geophys. Res.*, **100**, 13919-13926.

Wang, J., H.L. Cole, D.J. Carlson, E.R. Miller, K. Beierle, A. Paukkunen, and T.K. Laine, 2002: Corrections of humidity measurement errors from the Vaisala RS80 radiosonde --- Application to TOGA COARE data. *J. Atmos. Oceanic Technol.*, **19**, 981-1002.

Wexler, A., 1976: Vapor pressure formulation for water in range 0 to 100°C: A revision. *J. Res. Nat. Bur. Stand.*, **80A**, 775-785.

Zipser, E.J. and R.H. Johnson, 1998: Systematic errors in radiosonde humidities: A global problem? *Tenth Symposium on Meteorological Observations and Instrumentation*, Phoenix, Arizona, 11-16 January, 72-73.

Vaisala RS80 Bias Corrections

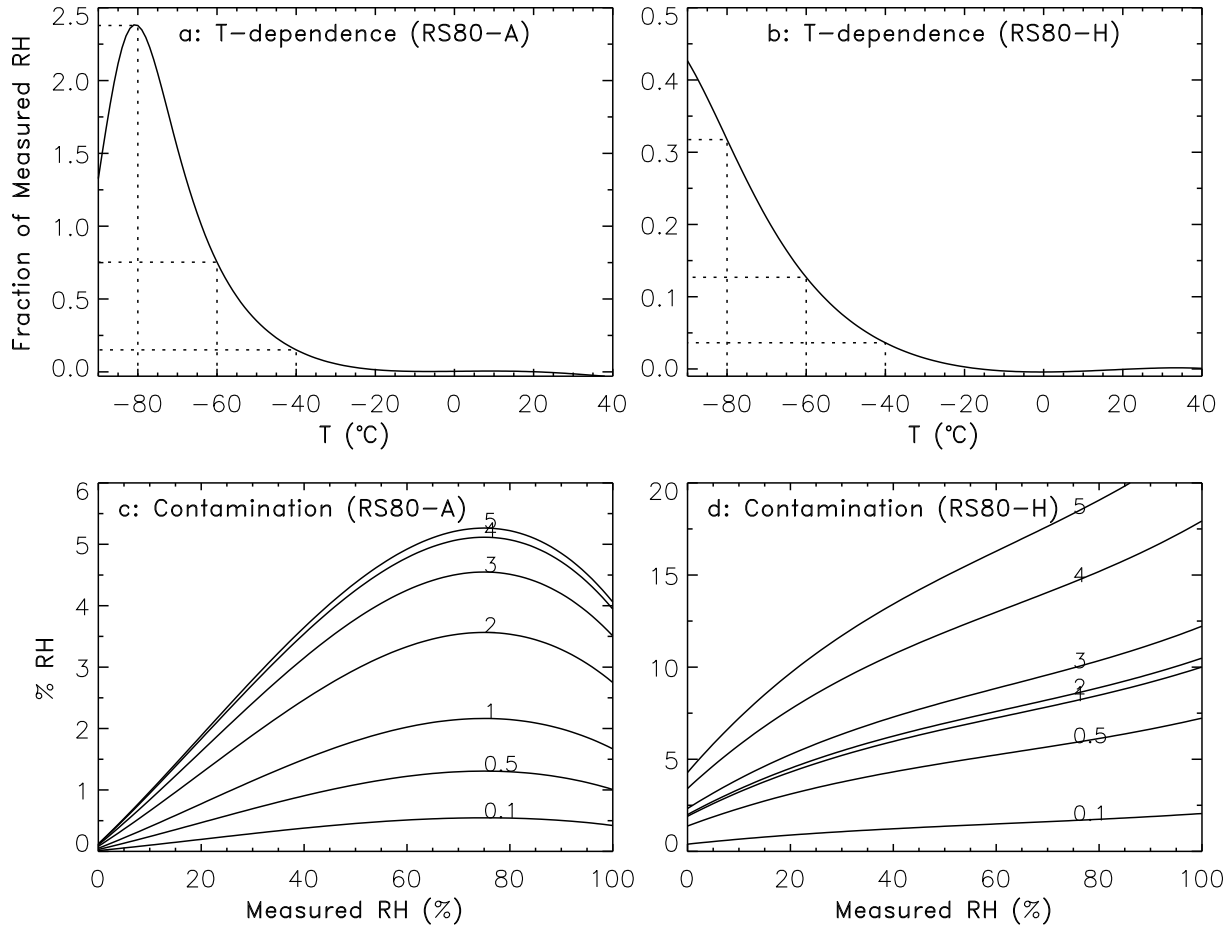


Figure 1: Corrections for the two primary dry-bias errors that affect Vaisala RS80-A (left) and RS80-H (right) radiosonde humidity measurements. Top panels show the correction for temperature-dependence (TD) error as a function of temperature, expressed as a fraction of the measured humidity. Bottom panels show the correction for contamination error in %RH, as a function of the measured humidity for radiosondes of the labeled ages (yrs). Note that the RS80-A and RS80-H corrections have different scales.

Time-Constant for Vaisala Radiosonde Humidity Sensors

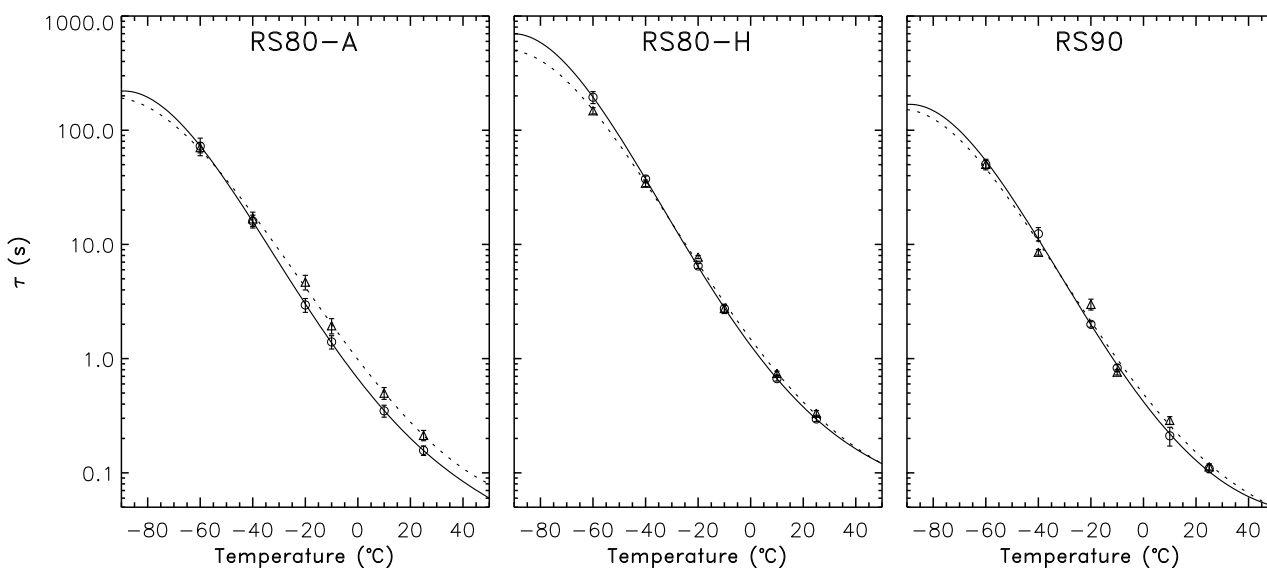


Figure 2: Mean and standard deviation of the 63% response time (τ) as a function of temperature for Vaisala RS80-A, RS80-H, and RS90 radiosonde humidity sensors. Curves show polynomial fits to the mean values for conditions when the RH is either increasing (circles; solid curve) or decreasing (triangles; dashed curve). Artificial points were added at -90°C and $+50^{\circ}\text{C}$ to constrain the fits to reasonable and conservative values outside the temperature range of the measurements.

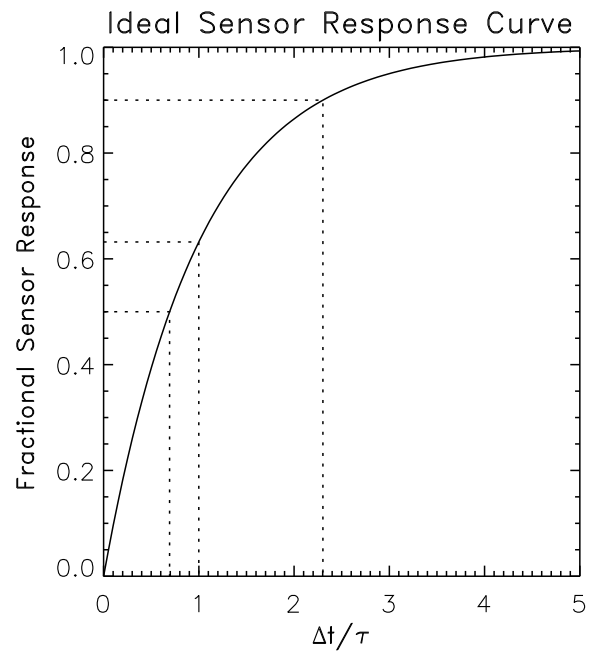


Figure 3: Fractional response of an ideal humidity sensor as a function of time in units of the time-constant (τ), given by $1 - e^{-\Delta t/\tau}$.

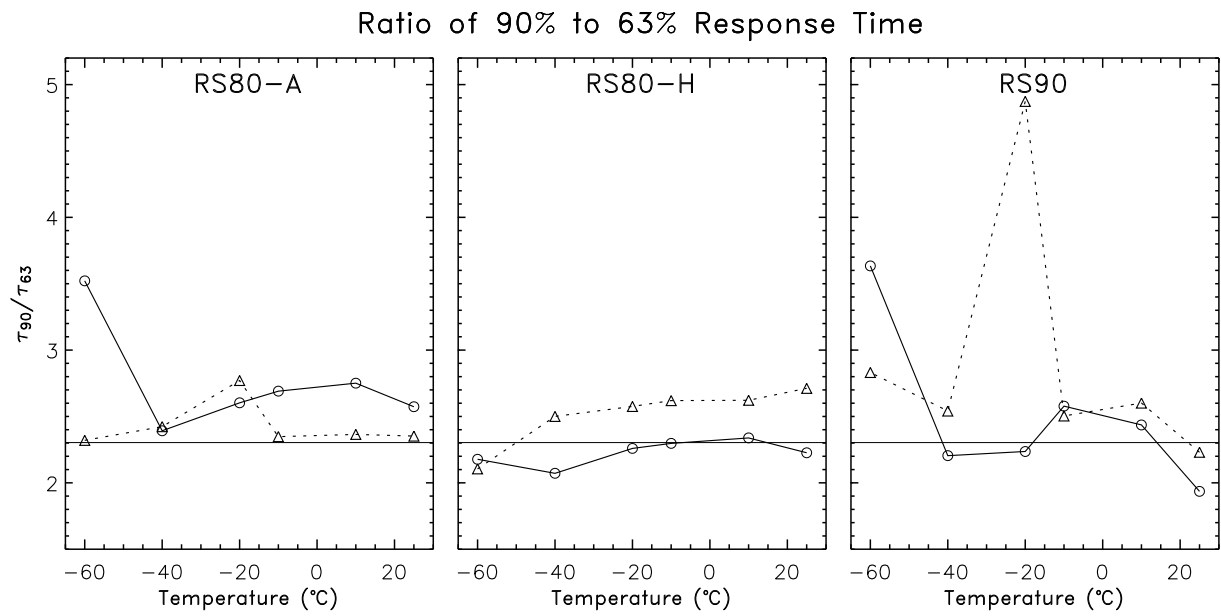


Figure 4: Ratio of the mean 90% to 63% response times from Table 1, for conditions of increasing RH (solid; circles) and decreasing RH (dashed; triangles).

Temperature Dependence of Time-lag Error

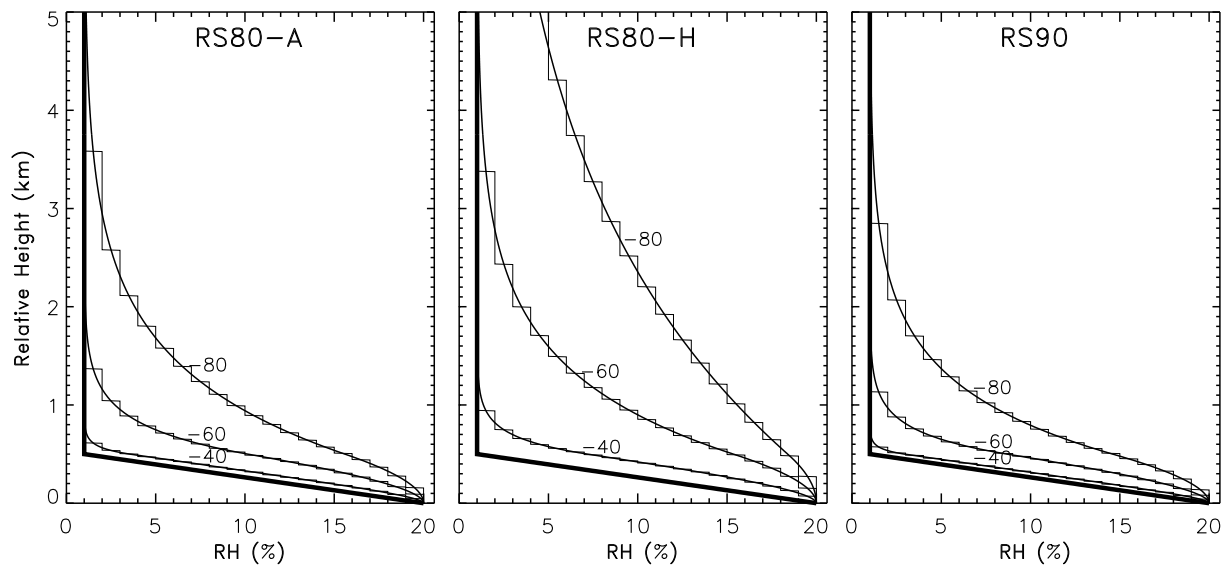


Figure 5: Simulated humidity measurements as a function of height (smooth curves at labeled temperatures) for a specified linear decrease in the “ambient” humidity (bold curve). The assumed radiosonde ascent rate is 5 m s^{-1} , and the temperature ($^{\circ}\text{C}$) is held constant. Stairsteps show the simulated measurements if the data resolution was 1 %RH, as is common.

Time-lag Correction Procedure

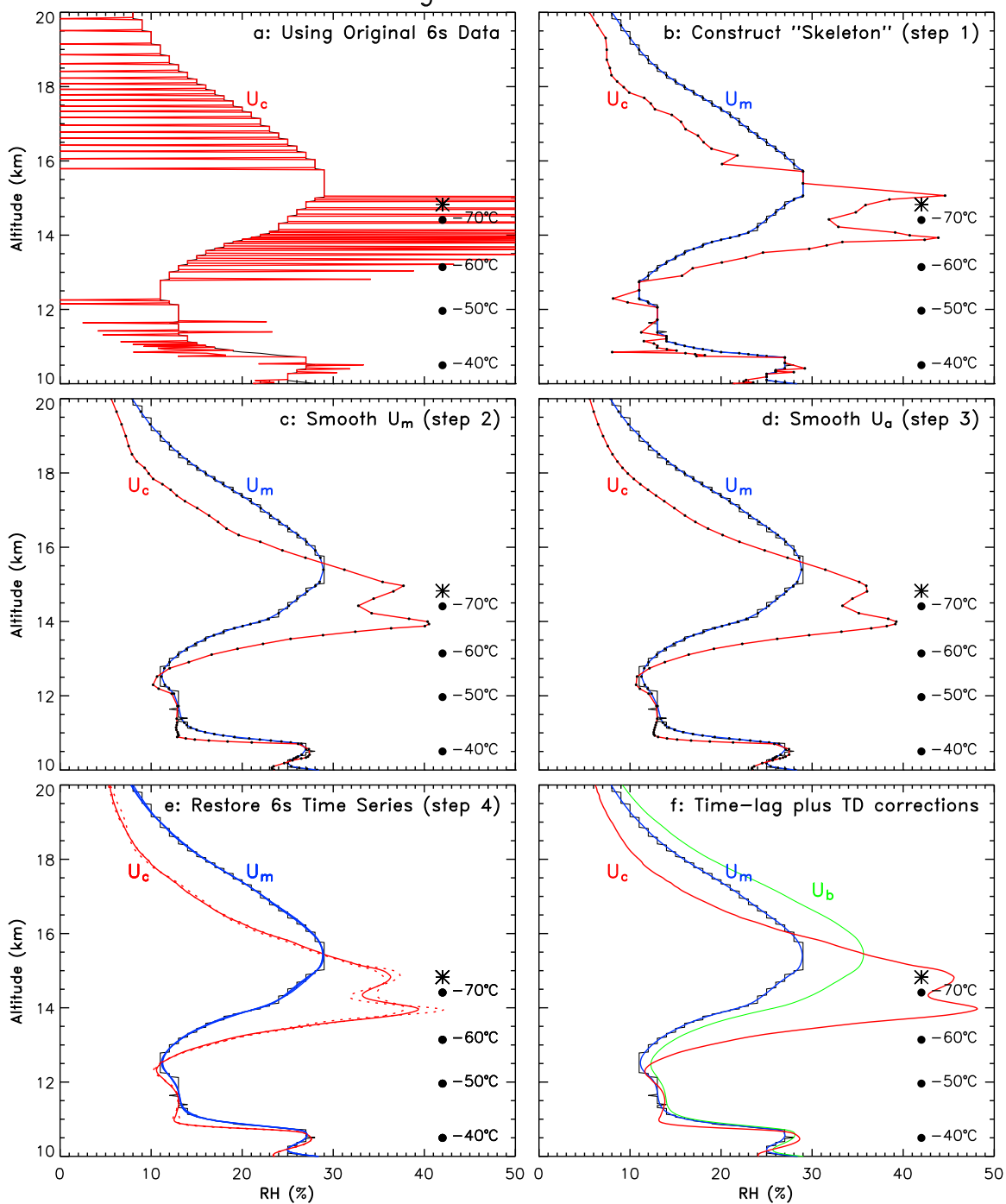


Figure 6: Panels b-e illustrate the steps in the time-lag correction procedure discussed in the text, as applied to the UT/LS portion of a NWS 6s humidity sounding. Curves are: original RH profile (black stairsteps), smoothed RH profile (blue, U_m), and the RH profile corrected for time-lag error by applying Eq. (4) to U_m (red, U_c). Black dots in panels b-d show the “skeleton” points used in the calculation, whereas the full 6s time series is shown in the other panels. Dashed curves in panel (e) show the corrected profile for different smoothing tolerance parameters. Panel (f) shows the final corrected profile when the TD correction (green, U_b) is applied prior to the time-lag correction. The asterisk is the tropopause altitude.

Comparison of Corrected RS80-H and NOAA Hygrometer Profiles

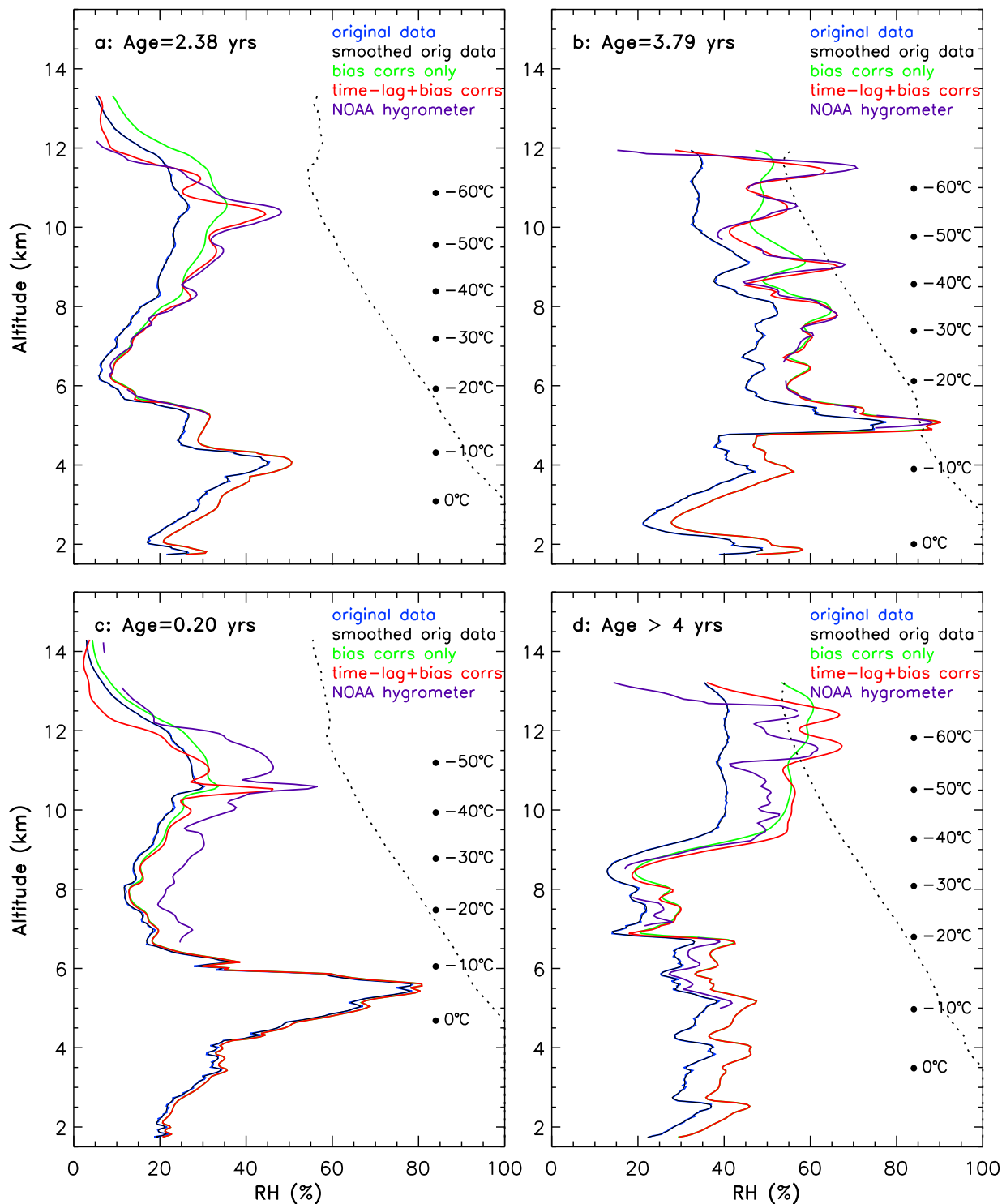


Figure 7: Comparison of four Vaisala RS80-H humidity profiles after correction for time-lag, TD, and contamination errors (red) with simultaneous measurements from the NOAA/CMDL cryogenic hygrometer (purple). Other curves are: original radiosonde data (light blue, beneath black), smoothed radiosonde data (black), radiosonde data corrected for only the TD and contamination dry-bias errors (green), and the ice-saturation curve (dashed). Panels are labeled with the age of the radiosonde at launch, used to calculate the contamination correction from W02.

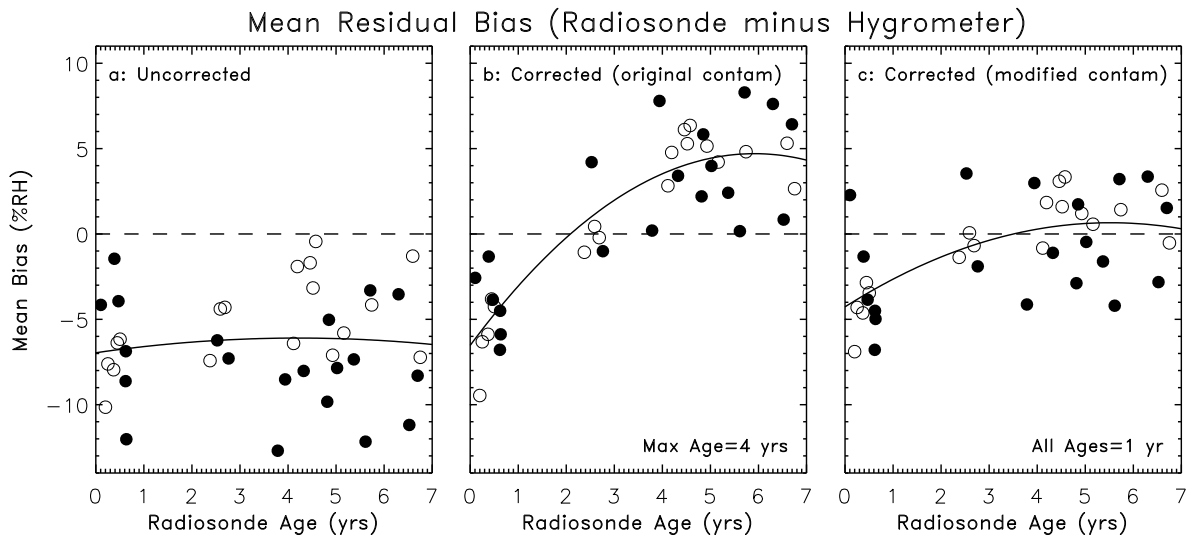


Figure 8: Mean (profile-average) RH difference between the RS80-H and hygrometer measurements for each of the 40 soundings, as a function of the radiosonde age. The mean bias is shown for the original RS80-H data (a), and after correction for time-lag, TD, and contamination errors (b and c). The original contamination correction from W02 was used in panel (b), except that a maximum age of 4 years was used to calculate the correction for older radiosondes. The modified contamination correction was used in panel (c), where a constant age of 1 year was used to calculate the correction (see justification in Appendix C). Open circles indicate that the mean RH measured by the hygrometer was $<30\%$ RH, and filled circles indicate that the mean RH was $>30\%$ RH. The solid curve is a polynomial fit for reference.

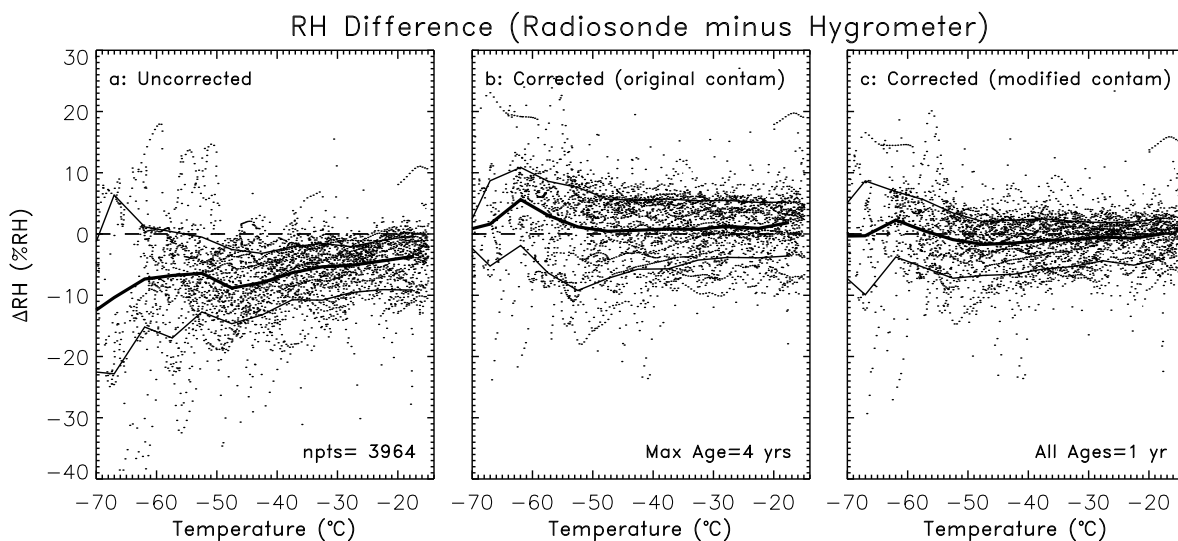


Figure 9: RH difference between corresponding RS80-H and hygrometer measurements, shown as a function of temperature for the original RS80-H data (a), and after correction for time-lag, TD, and contamination errors (b and c). The original contamination correction from W02 was used in panel (b), and the modified contamination correction from Appendix C was used in panel (c). Data are included if the temperature is below -15°C and the altitude is below the tropopause. Curves are the mean in 5°C temperature bins (bold), and the 68th percentile above and below the mean.

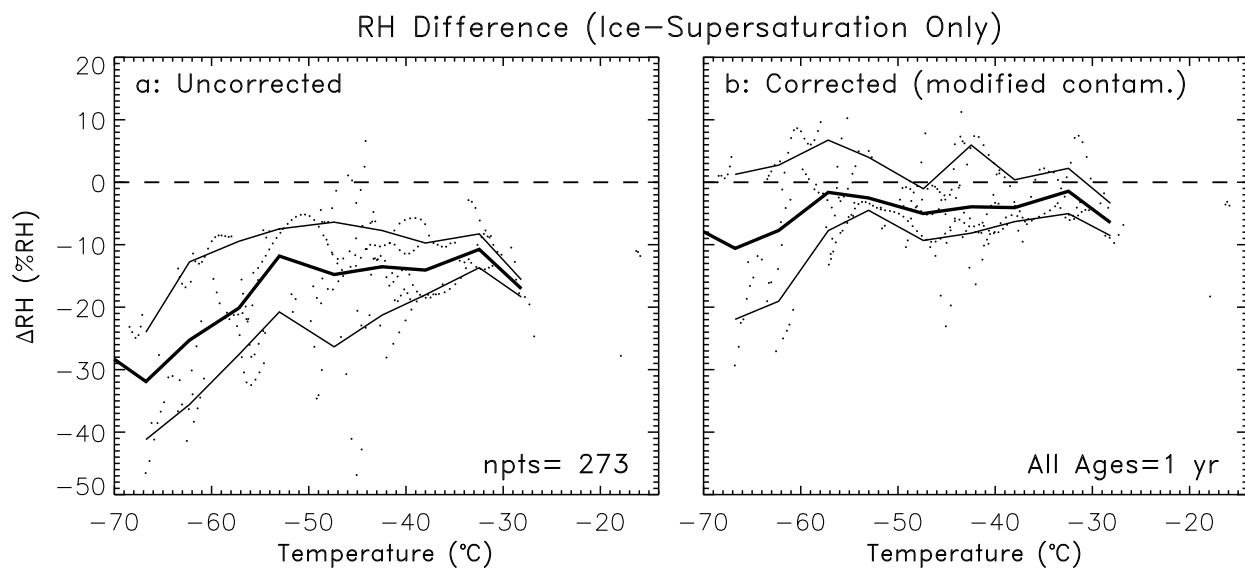


Figure 10: RH difference between RS80-H and hygrometer measurements before and after correction, as in Fig. 9, but for only those instances when the RH measured by the hygrometer exceeds ice-saturation.

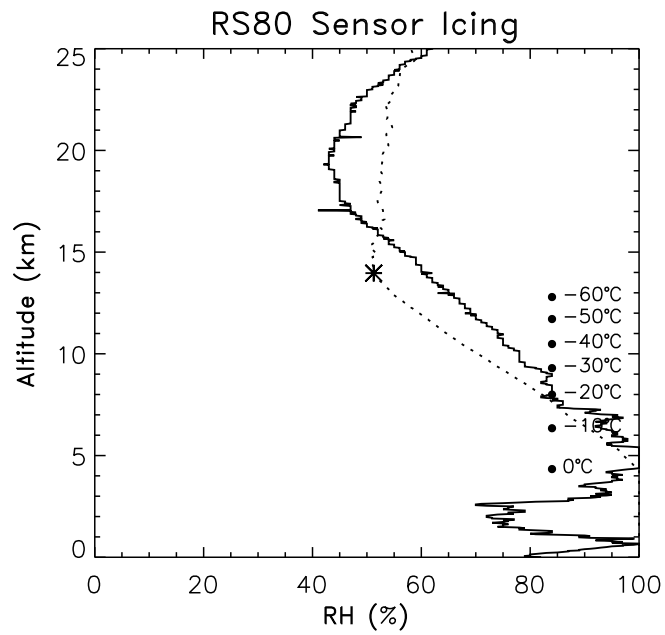


Figure 11: RS80-H humidity sounding from the Miami NWS site that illustrates sensor icing caused by exposure to supercooled liquid water. Shown are the original data (solid curve), ice-saturation (dashed), and the tropopause (asterisk). Corrected data are not shown because it is as erroneous as the original data.

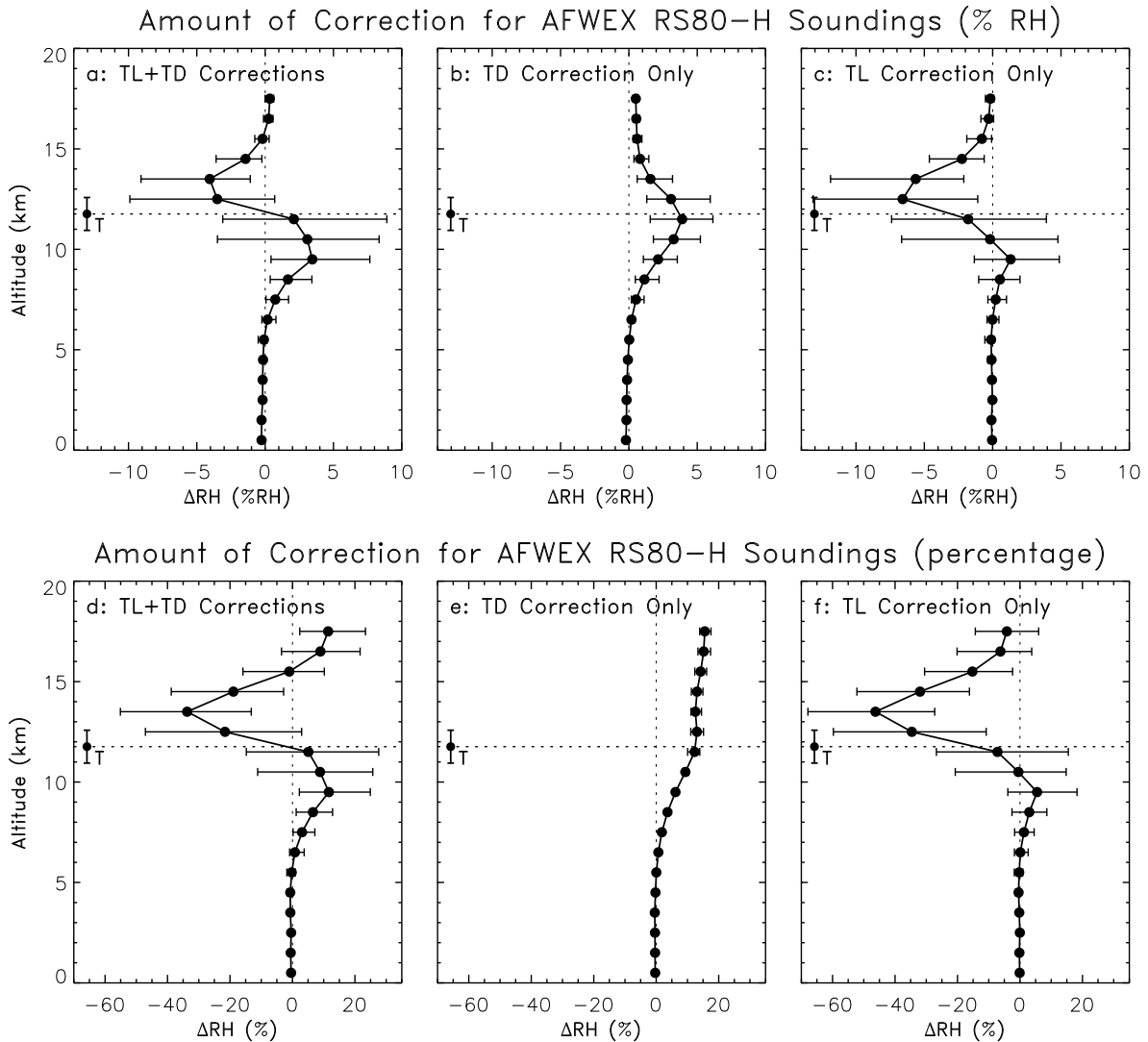


Figure 12: Amount of correction as a function of altitude for 125 RS80-H humidity soundings acquired during AFWEX in Dec. 2000 at the ARM Oklahoma site. Dots show the mean difference between the corrected and uncorrected data in 1 km altitude increments, and horizontal bars show the 68th percentile of the distribution above and below the mean. Top panels give the amount of correction in units of %RH for the total correction (TD + time-lag; panel a), and for the individual contributions from the TD correction (panel b) and the time-lag correction (panel c). Bottom panels show the amount of correction as above, but as a percentage of the measured RH (% , not %RH). Vertical bars show the mean and standard deviation of the tropopause altitude.

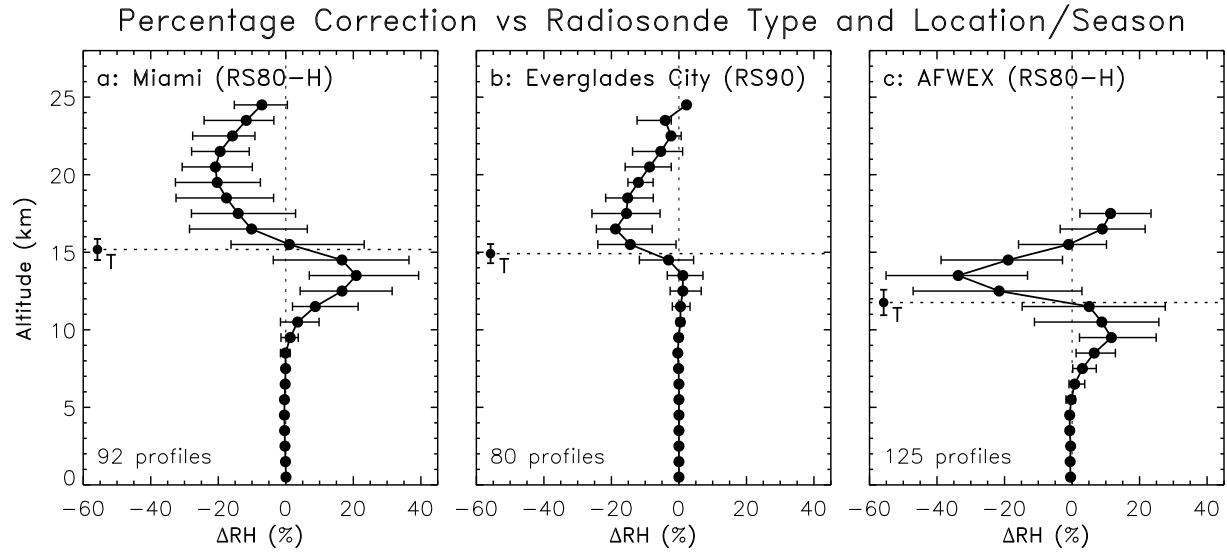


Figure 13: Altitude profiles of the amount of correction as a percentage of the measured RH, for an RS90 dataset and two RS80-H datasets (including AFWEX from Fig. 12d). Panels (a) and (b) are from the July 2002 NASA/CRYSTAL-FACE experiment in south Florida. The time-lag correction was applied to all soundings, and the TD correction was applied to the RS80-H soundings. All RS80-H radiosondes were produced after June 2000, so no contamination correction is applied. Symbols are the same as in Fig. 12.

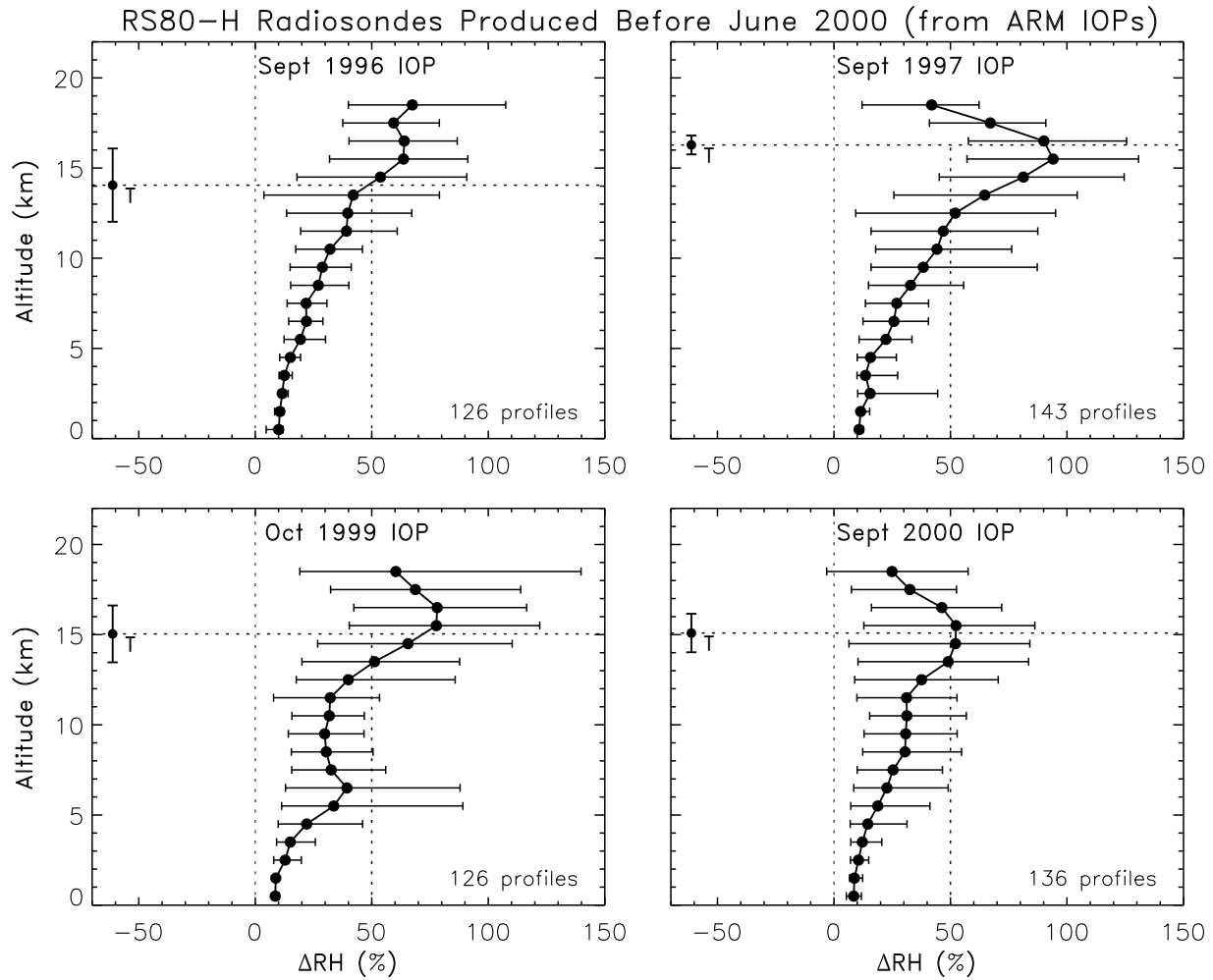


Figure 14: Altitude profiles of the amount of correction as a percentage of the measured RH, for 4 ARM Water Vapor IOPs that used RS80-H radiosondes produced before 1 June 2000. The time-lag, TD, and modified contamination corrections were applied. Symbols are the same as in Fig. 12, with an additional reference line at $\Delta RH = 50\%$.

Derivative-Based Smoothing Algorithm

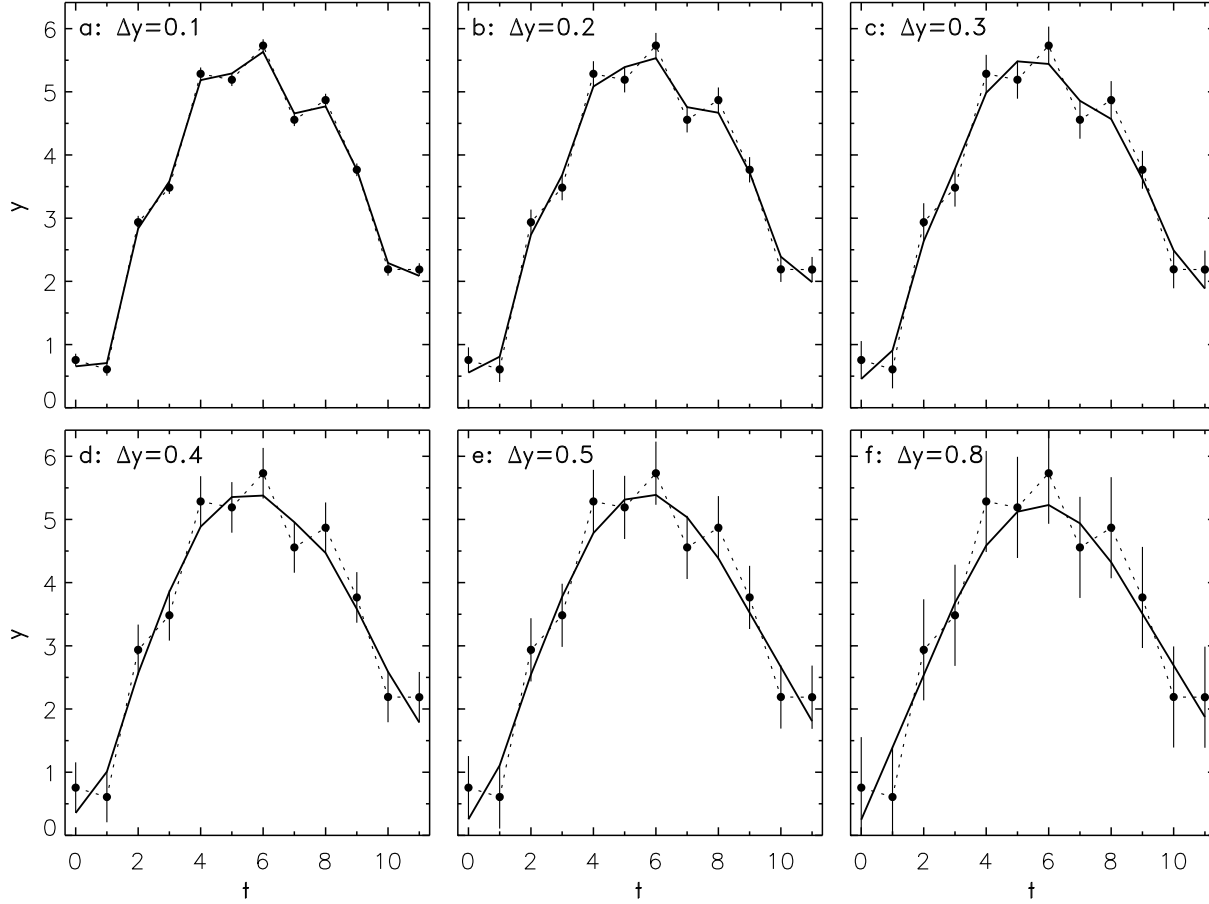


Figure B1: Sensitivity of the smoothing algorithm to the smoothing tolerance parameter Δy , for independent variable t . The dots and the dashed curve show the original (unsmoothed) data, and vertical bars show the allowable smoothing range $\pm \Delta y$. The solid curve is the solution that minimizes the third derivative while keeping all points within the specified tolerance.

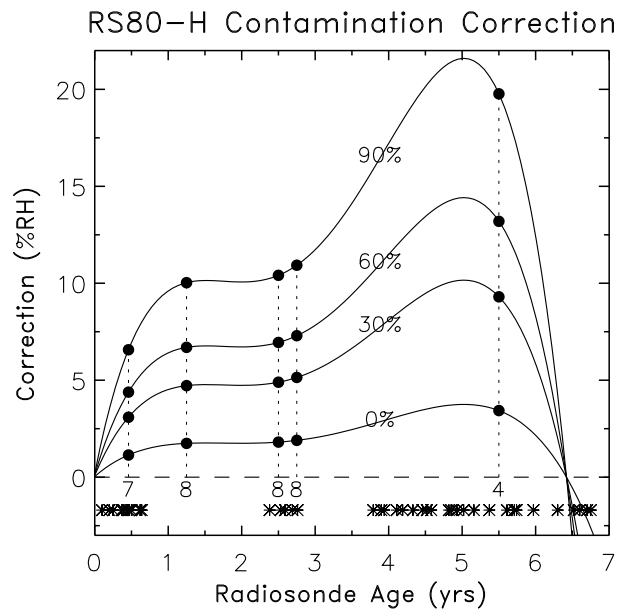


Figure C1: RS80-H contamination correction as a function of radiosonde age at +20°C, from W02. Curves show the correction (%RH) for the four labeled values of the measured RH. Dots and vertical dashed lines indicate the ages of the radiosondes that were tested by Vaisala and used to derive the contamination correction (number of radiosondes tested is also indicated). Asterisks show the ages of the 40 RS80-H radiosondes in the NOAA dataset.

Table 1

Mean 63% and 90% response time measurements for Vaisala radiosonde humidity sensors (τ), given as a function of temperature (T) and whether the RH is increasing (I) or decreasing (D). The standard deviation of the measurements is given as a fraction of the mean (σ/τ).

Sensor	T (°C)	τ_{63} (I)	τ_{63} (D)	τ_{90} (I)	τ_{90} (D)	$\frac{\sigma_{63}}{\tau_{63}}$ (I)	$\frac{\sigma_{63}}{\tau_{63}}$ (D)	$\frac{\sigma_{90}}{\tau_{90}}$ (I)	$\frac{\sigma_{90}}{\tau_{90}}$ (D)
RS80-A	-60	72.500	70.576	255.306	163.747	0.176	0.103	0.144	0.083
	-40	15.982	16.768	38.229	40.632	0.129	0.143	0.143	0.130
	-20	2.950	4.678	7.678	12.961	0.139	0.146	0.125	0.158
	-10	1.400	1.943	3.767	4.562	0.134	0.153	0.137	0.156
	10	0.349	0.499	0.960	1.180	0.120	0.118	0.105	0.111
	25	0.157	0.213	0.404	0.501	0.096	0.103	0.082	0.108
RS80-H	-60	194.537	148.205	423.568	311.980	0.120	0.062	0.064	0.104
	-40	37.414	34.370	77.511	85.933	0.064	0.066	0.103	0.076
	-20	6.479	7.758	14.638	19.979	0.049	0.032	0.075	0.029
	-10	2.742	2.748	6.299	7.198	0.095	0.069	0.099	0.080
	10	0.668	0.743	1.562	1.948	0.048	0.044	0.040	0.037
	25	0.296	0.333	0.659	0.903	0.051	0.054	0.044	0.058
RS90	-60	50.321	50.317	182.867	142.464	0.083	0.106	0.346	0.120
	-40	12.381	8.540	27.298	21.699	0.135	0.056	0.187	0.055
	-20	1.996	2.991	4.463	14.576	0.054	0.109	0.074	0.190
	-10	0.829	0.762	2.137	1.908	0.066	0.056	0.101	0.061
	10	0.211	0.288	0.514	0.749	0.187	0.077	0.457	0.111
	25	0.109	0.113	0.211	0.252	0.080	0.063	0.070	0.068

Table 2

Coefficients for polynomial fits to the mean 63% response time as a function of temperature, $\tau(T)$, when the RH is either increasing (I) or decreasing (D).

$$\tau(T) = 10^{P(T)}, \text{ where } P(T) = a_0 + (a_1 \cdot T) + (a_2 \cdot T^2) + (a_3 \cdot T^3) + (a_4 \cdot T^4)$$

Sensor	RH	a_0	a_1	a_2	a_3	a_4
RS80-A	I	-1.75420e-1	-2.97467e-2	1.71521e-4	8.21223e-7	-1.44814e-8
	D	-7.32613e-3	-3.00662e-2	1.07110e-4	1.37684e-6	-4.28963e-9
RS80-H	I	1.15175e-1	-3.10791e-2	1.96010e-4	9.56061e-7	-1.46019e-8
	D	1.70504e-1	-3.08027e-2	1.45599e-4	1.15187e-6	-8.91805e-9
RS90	I	-3.77053e-1	-3.02416e-2	2.05624e-4	1.28424e-6	-1.29289e-8
	D	-3.09810e-1	-2.90791e-2	1.62583e-4	9.78907e-7	-1.11286e-8

Table 3

Factors $F(T)$ that adjust the polynomial fits shown in Figure 2 to compensate for curve-fit error and to decrease the time-constant values by one standard deviation at the measurement temperatures.

Sensor	RH	-90°C	-60°C	-40°C	-20°C	-10°C	+10°C	+25°C	+50°C
RS80-A	I	1.000	0.822	0.880	0.843	0.882	0.875	0.906	1.000
	D	0.995	0.938	0.776	0.947	0.819	0.870	0.898	1.002
RS80-H	I	1.000	0.879	0.936	0.965	0.892	0.952	0.952	0.999
	D	1.004	0.922	0.928	1.100	0.824	0.940	0.983	0.992
RS90	I	1.011	0.854	0.963	0.951	0.880	0.780	0.979	0.987
	D	0.990	0.973	0.766	1.255	0.725	1.019	0.889	1.008